Design Considerations for a Mars Highland Helicopter

Larry A. Young[1], Jeff Delaune[2], Wayne Johnson[3], Shannah Withrow-Maser[4], Haley Cummings[5], Evgeniy Sklyanskiy[6], Jacob Izraelevitz[7], Aaron Schutte[8], Abigail Fraeman[9], Raghav Bhagwat[10]

Abstract

Mars is sharply divided into the relatively low-lying northern hemisphere, filled with plains, to the higher-elevation, rugged, southern hemisphere. All landers sent so far to Mars have only landed on the plains of the northern hemisphere. Access to the Martian Highlands would present an opportunity to acquire unique insights into the early geologic history of Mars. But landing on the Martian highlands presents many engineering challenges. A new approach has recently been proposed to consider the use of mid-air deployment, during the final subsonic stages of entry, descent, and landing, of a small rotorcraft from the aeroshell. The rotorcraft would enter a powered descent state (rotors would be spun to full speed at moderate collectives) after aeroshell release until reaching a modest altitude above the ground where the vehicle would pullout to level flight. After completing this initial EDL mid-air-deployment and landing, the rotorcraft, which would be capable of solar-electric recharging, would recharge over the course of a few days until ready for subsequent flight sorties to explore the highlands. This overall vehicle/mission concept is called the Mars Highland Helicopter. The paper will next demonstrate that a key necessary condition – efficient hover and forward flight under the much thinner atmospheric conditions of the highlands (0.01 kg/m3 vs. 0.015 kg.m3 for the Ingenuity Mars Helicopter Technology Demonstrator at Jezero Crater) – is indeed possible. This paper considers a number of EDL release/deployment strategies to minimize deployment aeroloads and maximize controllability during release from the EDL backshell. This mid-air-deployment discussion will be followed by a general analytical treatment of a Mars rotorcraft entering fully-powered descent and then forward flight cruise.

[1] Associate Fellow; Aeromechanics Office, NASA Ames Research Center, Moffett Field, CA
[2] Robotics Technologist, NASA Jet Propulsion Laboratory, Pasadena, CA
[3] Fellow; Aeromechanics Office, NASA Ames Research Center, Moffett Field, CA
[4] Member; Aeromechanics Office, NASA Ames Research Center, Moffett Field, CA
[5] Member; Aeromechanics Office, NASA Ames Research Center, Moffett Field, CA
[6] NASA Jet Propulsion Laboratory, Pasadena, CA
[7] NASA Jet Propulsion Laboratory, Pasadena, CA
[8] NASA Jet Propulsion Laboratory, Pasadena, CA
[9] NASA Jet Propulsion Laboratory, Pasadena, CA
[10] Student intern, Ohio State University, Aeromechanics Office, NASA Ames Research Center, Moffett Field, CA

Nomenclature

AGL	Above ground level
AMH	Advanced Mars Helicopter
CONOPS	Concept of operations
c	Speed of sound, m/s
C_{PL}	Lower rotor power coefficient
C_{PU}	Upper rotor power coefficient
C_{TL}	Lower rotor thrust coefficient
C_{TU}	Upper rotor thrust coefficient
D	Aeroshell/capsule diameter, m
EDL	Entry, Descent, and Landing
HIGE	Hover in ground effect
HOGE	Hover out of ground effect
MHH	Mars Highland Helicopter
MSH	Mars Science Helicopter
MHTD	Mars Helicopter Technology Demonstrator, aka "Ingenuity"
NDARC	NASA Design and Analysis of Rotorcraft software tool
R	Rotor radius, m
s/R	Rotor-to-rotor vertical spacing ratio with respect to rotor radius
s_D/R	Solar array vertical spacing from upper rotor with respect to rotor radius
V_D	Descent velocity, m/s
V_{Tip}	Rotor tip speed, m/s
V	Forward flight cruise velocity, m
VTOL	Vertical takeoff and landing
α_{shaft}	Rotor shaft angle, zero degrees when rotor axes are vertical, Deg.
$\theta_{0.75}$	Rotor collective, i.e. blade pitch angle at the seventy-five percent radial station, Deg.
μ	Forward flight advance ratio, $\mu = V/V_{Tip}$

Introduction

NASA has long pursued investigations into Mars helicopters and other Mars rotorcraft, Ref. 1. This work has culminated in the launch of the Ingenuity Mars Helicopter Technology Demonstrator (MHTD), which was developed as part of a joint Jet Propulsion Laboratory, NASA Ames, NASA Langley, and AeroVironment effort, Ref. 10. The exploration of the Martian highlands is of high scientific interest, Ref. 5. A mission concept to explore the Martian highlands by means of a Mars helicopter is currently being developed by a joint JPL and NASA Ames team, Ref. 2. This paper will focus on the vehicle design challenges for such a Mars Highland Helicopter (MHH). Chief among those challenges is developing mid-air-deployment concepts and concepts of operations (CONOPS) for the MHH.

Figure 1 presents temperature and atmospheric density trends as a function of altitude (AGL) for three different possible Mars landing sites. In order to successfully land at these sites, it is both necessary to design a Mars Highland Helicopter to descend/decelerate from an EDL ssytem aeroshell and to efficiently achieve level flight under these extreme conditions. The lower

temperatures and thinner atmosphere of Mars – and especially that of the Martian highlands – are challenging from both a design perspective as well as from a concept of operations perspective.
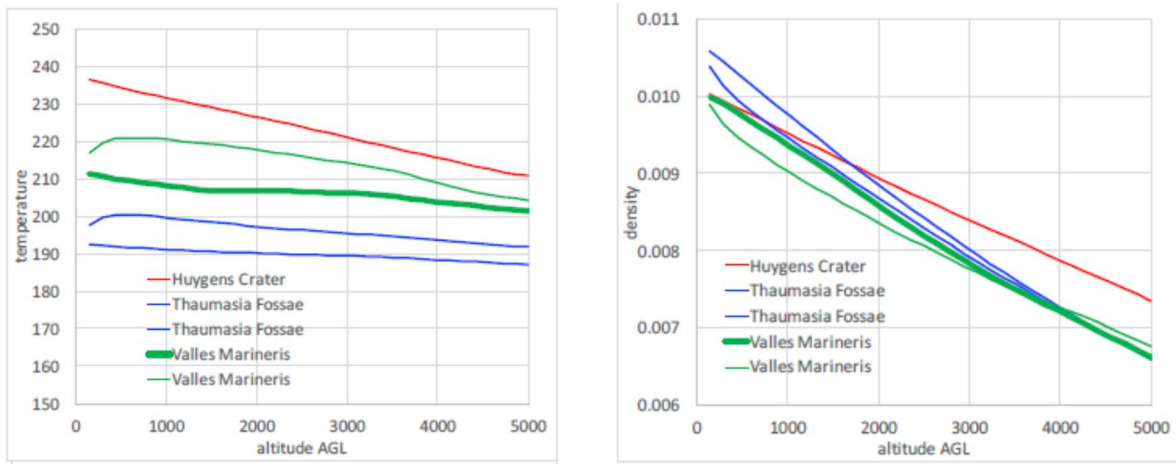

Figure 1. Atmospheric density (kg/m³) and temperature (Kelvin) as a function of altitude (meters) for three Mars landing sites

A notional mid-air deployment CONOPs for the MHH is outlined below:

1. Because of the ultra-lightweight nature of MHH, and EDL stowage/packaging volumetric considerations whereby the upper portion of the aeroshell is relatively unoccupied by hardware, a larger parachute could likely be accommodated to achieve lower subsonic descent terminal velocities at higher altitudes. (For example, a Mars Pathfinder-like aeroshell could potentially carry a Mars Science Laboratory (MSL)-class parachute.)

2. Prior to the release of the heat shield, the MHH rotors would be spun-up to full rpm for descent. These rotors would likely be spun-up at 'flat pitch' or zero rotor control system collective thereby minimizing transient/unsteady loading of the rotor blades due to high levels of flow recirculation in the tight confines of the aeroshell interior. This pre-heat-shield-release spin-up will likely be required as the rotor blades of any Mars rotorcraft are large, lightweight, and have low non-rotating stiffness. Because Mars rotor blades are ultralight-weight they tend to have low structural stiffness. The centrifugal stiffening of the blades stemming from their being spun to their full rpm before heat shield release will ensure that they will be able to withstand the aerodynamic loads during heat shield release and the subsequent vehicle release from the back shell. This pre-release (heat shield) rotor spin-up in the close confines of the sealed aeroshell are explored later in this paper. Future work will consider the spin-up of the blades post-heat-shield-release.

3. There are several different options that will need to be explored in depth to determine the best means of releasing and 'pushing off' the vehicle from the back shell. These range from mechanical designs for telescoping booms, to scissor-like trusses, to spring-actuated devices to mechanically push the MHH out of the back shell to some position that the vehicle can freely and safely drop below the back shell. There is also an aero-vehicle option whereby the rotors are designed to be able to generate "negative thrust" by setting

negative rotor collective such that the vehicle "propels" itself out of the back shell. Combinations of these different options may also be required to minimize risk during MHH release/deployment. The "negative thrust" option will be explored later in this paper.

4. Upon release and safe clearance from the back shell, the MHH will increase collective from negative or near zero collective to the maximum collective setting so as to arrest vehicle descent velocity (from its initial velocity of ~30m/s). This may require overspeeding the rotors to further enable maximum deceleration. Nominal tip Mach number ranges between 0.7-0.8 for hover and forward flight. Overspeeding the rotors up to a tip Mach number of 0.85 was prescribed in the current studies. This maximizes rotor thrust during descent. Cyclic control inputs would be inparted to trim the rotors (shifting the vehicle to a "nosedown" attitude) and begin picking up some forward horizontal speed. This nosedown attitude would be only be for a short period of time to clear the vehicle from the path of the descending aeroshell and parachute. The vehicle would then be returned to a straight-down, axial-flow descent profile to maximize deceleration to arrest vehicle descent at, or above, the minimum design target altitude, i.e. ~3.5km.

5. As nominal cruise altitude is approached, the vehicle is trimmed via cyclic rotor control to pullout to level flight.

6. On the basis of guidance, navigation, and control (GNC) avionics, sensors, and site selection methodologies, the vehicle slows to an approach profile and an initial VTOL landing is made at the target site.

This mid-air-deployment CONOPs will be informed and updated by the work that follows and future planned work on the MHH mission concept and vehicle design.

Initial Release from Entry, Descent, and Landing System

EDL CFD Prediction Using a "Rotorcraft" Mid-Fidelity Tool

Figure 2 is a representative mid-fidelity CFD flow field (with body surface pressures) of the Mars Pathfinder EDL combination of gap-band parachute, aeroshell back shell, and tetrahedral lander. Not modeled in this figure is the parachute cords/lines, tethers, and 'bridle.' The parachute is modeled as a finite-thickness shell (thicker in actuality than the Pathfinder parachute) that is rigid and not distorted or aeroelastically deflected by the parachute aeroloads.
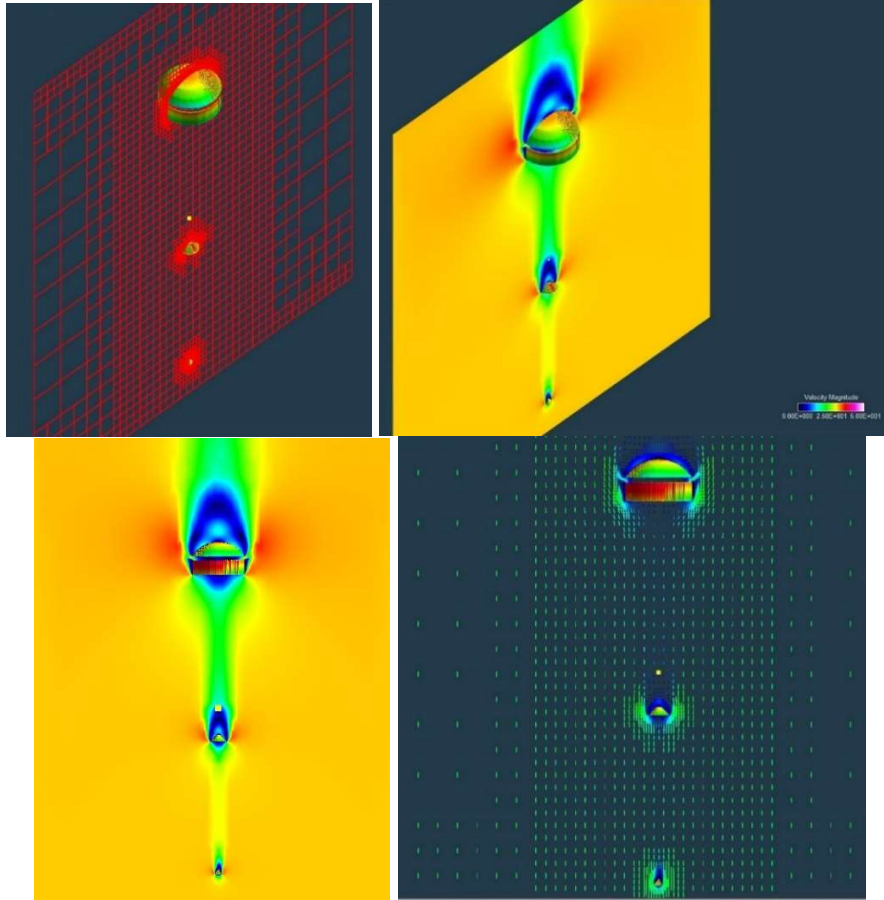
Figure 2. RotCFD modeling of the final terminal descent velocity of the Mars Pathfinder-like configuration with the heat shield separated and the lander deployed on a bridle
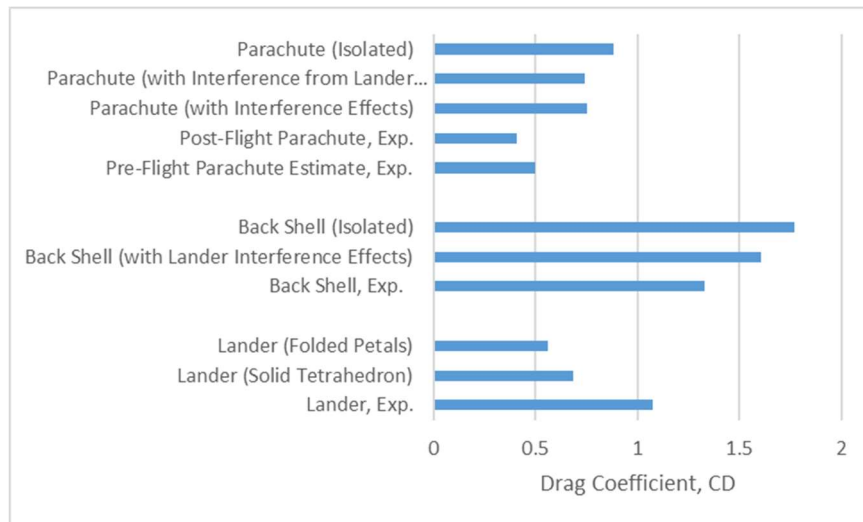

Figure 3. Predicted versus experimental values of drag coefficient for Mars Pathfinder EDL system (coarse grids)

RotCFD is a mid-fidelity computational fluid dynamics (CFD) tool tailored for rotorcraft applications, Refs. 7-9. RotCFD predictions of drag coefficients of the Mars Pathfinder EDL system components are shown in Fig. 3. The predictions are only fair with respect to the experimental values. In general, this is because of the coarseness of the grids. The back shell drag coefficient prediction is perhaps the most accurate of the RotCFD predictions. There are a number of reasons why these predictions do not match the experimental values better. In the case of the parachute, use of a rigid, large finite-thickness shell to represent the parachute probably had a significant impact. In the case of the lander, the lack of a high fidelity CAD geometry to generate satisfactory grids, plus the uncertainties of how, or whether, to model cutouts in the tetrahedral lander that could, or could not, allow flow into the interior of the lander, also likely had an impact. And, finally, in the case of the back shell, a lack of high fidelity CAD geometry, including the exposed backshell interior, was not available and likely also had an impact. In all cases, RotCFD is not well-suited, by virtue of being a mid-fidelity tool, of accurately modeling three-dimensional boundary layers and seperated flow. Nonetheless, it is anticipated that the backshell modeling is sufficient to examine the MHH pre- and post-release (from the backshell) aerodynamics.

Recognizing the ultra-lightweight nature of Mars Highland Helicopter designs, and consideration of vehicle stowage constraints in the aeroshell, will result in increased available volume in even a Pathfinder-like aeroshell to perhaps accommodate a larger Mars 2020-class parachute. This would even further improve the ballistic coefficient of an EDL system for a Martian highlands mission.

CFD Prediction of Rotor Spin-Up Pre-Release

The analysis in this section assumes that the EDL system aeroshell is vented, perhaps via valving at the bottom of the parachute cannister, into the Martian atmosphere after parachute release and low subsonic descent speeds are achieved.

A major design and operational consideration is how to best spin-up and achieve the nominal thrust of the rotors prior to release from the EDL system back shell. Two basic approaches suggest themselves. First, the rotor spin-up could occur while still in the sealed aeroshell. Second, the rotor spin-up – and subsequently pulling rotor collective – could occur while suspended from/in the back shell after heat shield separation. Spin up inside the aeroshell has the advantage in that it does not expose the ultra-lightweight and relatively low-stiffness rotor blades to the brunt of the descent velocity flow field. However, spinning up the blades inside the aeroshell might result in very unsteady velocities in the close confines of the aeroshell interior. Alternatively, spinning up the rotors after the heat shield has been released might still be viable because of the large region of upwind stagnation flow just below the back shell opening (and the MHH rotors). Again, as in the case of spinning up inside the sealed aeroshell, the principal concern about spinning up the rotors after the heat shield is released is that transient and/or other unsteady velocities – and, therefore, blade aero-loading – may be too severe to resist either from an aeroelastic deflection and/or strength perspective.

Note that the 2m diameter rotors studied in the following discussion are simply geometrically scaled from an earlier 1.21m diameter coaxial helicopter conceptual design, sized for flight over the Martian highlands. This smaller design will be discussed at the end of this paper as an alternate configuration to the larger 2m diameter coaxial rotor configuration. The 2m diameter rotor was selected as being the largest rotor that could fit within a Mars Pathfinder aeroshell without undergoing significant folding, telescoping, or canting. (Such folding, telescoping, and canting of

mechanical components, particularly rotating components such as the rotor blades, is not really consistent with the rapid unstowing/deploying of a vehicle, including rotor spin-up and increasing rotor collective, required for MHH mid-air-deployment.) As will be discussed in detail later, choosing a 2m diameter rotor size still presents additional mechanical challenges such as perhaps being forced to adopt a smaller rotor-to-rotor vertical spacing than optimal (or coming up with a complex telescoping rotor mast to increase that rotor-to-rotor spacing upon vehicle release from the back shell.)

Figure 4 is an extreme example of the classic "rotor in a box" flow recirculation interference effect problem. Therefore, the predicted results that follow must be considered very preliminary in nature until some sort of validation against other, higher fidelity analyses or experimental data is performed.

(a)

(b)
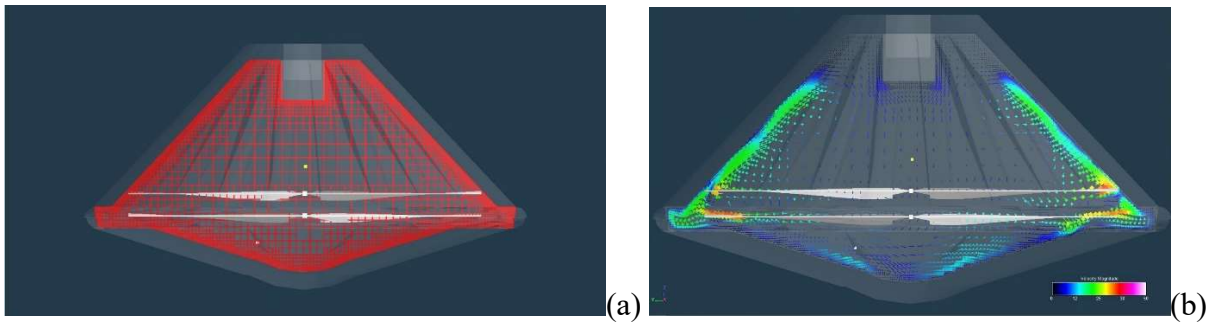
Figure 4. Flow field predictions of rotor spin-up while still in sealed aeroshell: (a) grid and (b) velocity vectors at collective = 0 Deg.

Figure 5a-b presents thrust and torque coefficient predictions for the coaxial rotors spinning in the sealed aeroshell. One of the key features of the predicted thrust levels is an exhibition of a possible bi-stable, multi-state thrust level for the rotors, particularly at higher thrust levels. This is a possible consequence of the flow field shifting between two different states as time (and the solution) progresses. Given the highly unsteady, recirculating flow in the aeroshell, this is perhaps not totally surprising. This will be examined more closely in future work.
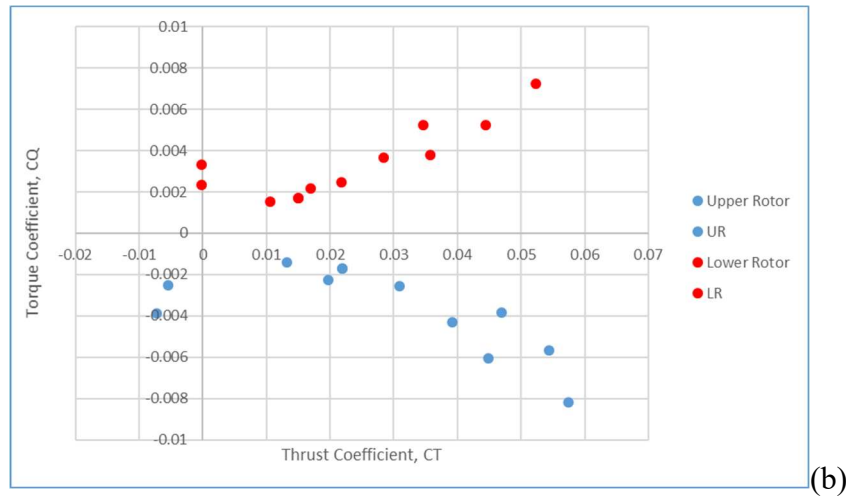

(a)

(b)
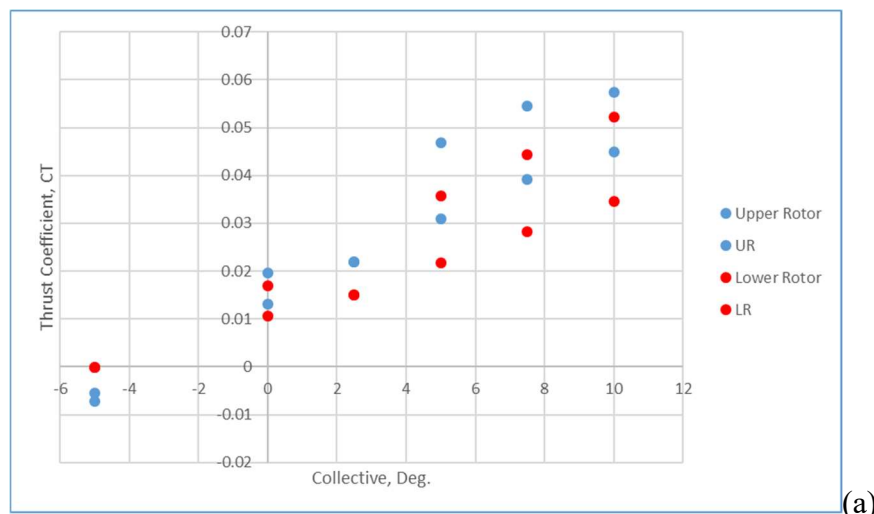
Figure 5. Rotor thrust and torque coefficient predictions of rotor spin-up and collective sweep to nominal thrust level while still in sealed aeroshell

Alternatively, the rotor could be spun up at flat-pitch (zero collective) within the sealed aeroshell, and then, after the heat shield is released, the rotor collective would be increased. Figure 6 presents an example of the flow field prediction for the MHH suspended from the backshell.
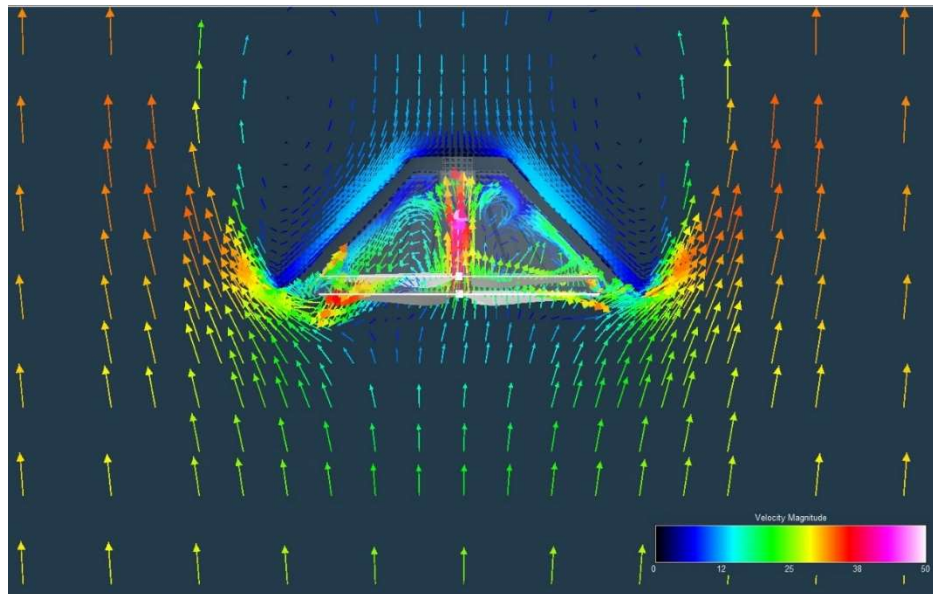

Figure 6. Flow field predictions of rotor spin-up and pulling collective while suspended in back shell after heat shield separation (full rpm at ten degrees collective)

CFD Prediction of Heat Shield and Backshell Separation

Figure 7 is a CFD prediction of the flow below and interior to an empty back shell. Conveniently, there seems to be large expanses of low velocity 'stagnation flow' in and below the back shell where one would want to spin up the MHH rotors. There is some fairly high radial flow predicted near the inner lip of the back shell but this, hopefully, should not result in too high blade aero loads.

It should be anticipated, though, that slight angles of attack of the backshell probably result in much higher recirculating flow in the back shell interior. This might be moderated by judicious venting of the back shell. Running nonzero angles of attack computationally and experimentally will be important and will be performed in future work.
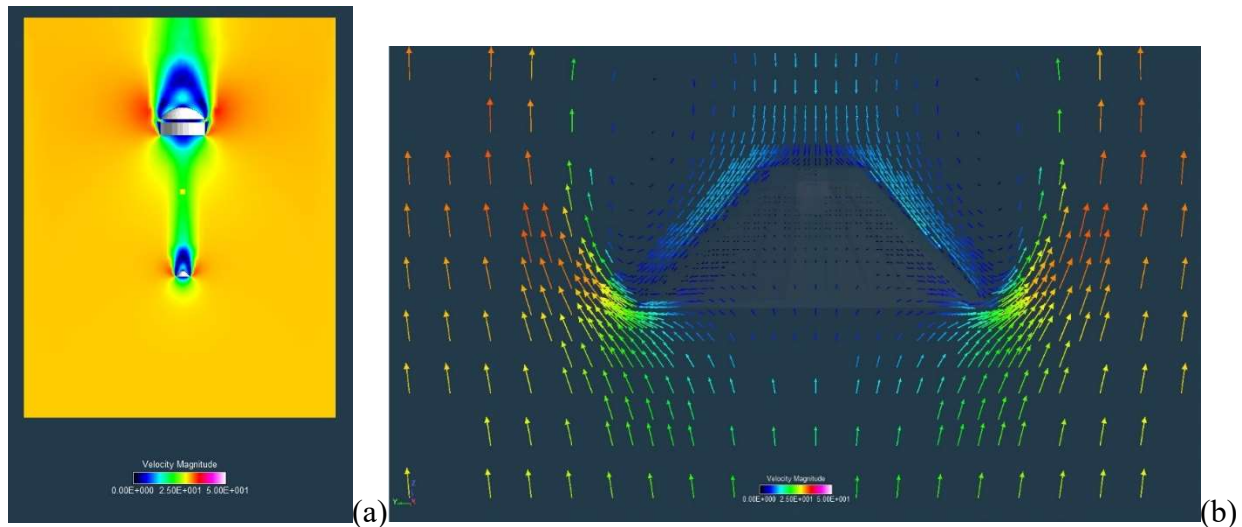
Figure 7. Flow field about (a) open backshell and parachute and (b) close-up of the open backshell at 30m/s descent velocity

Figure 8a-f illustrates the flow field surrounding a Mars Pathfinder-like EDL system capsule as the heat shield separates from the back shell at a descent velocity of 30 m/s. In this series of results there is no payload content in the aeroshell. In a later set of results, a set of coaxial rotors will be incorporated as a payload package in the capsule; these rotors will be spun up with resulting rotor downwash influencing the interior and exterior flow field. These are quasi-steady flow predictions; the back shell is not moving in the simulations.
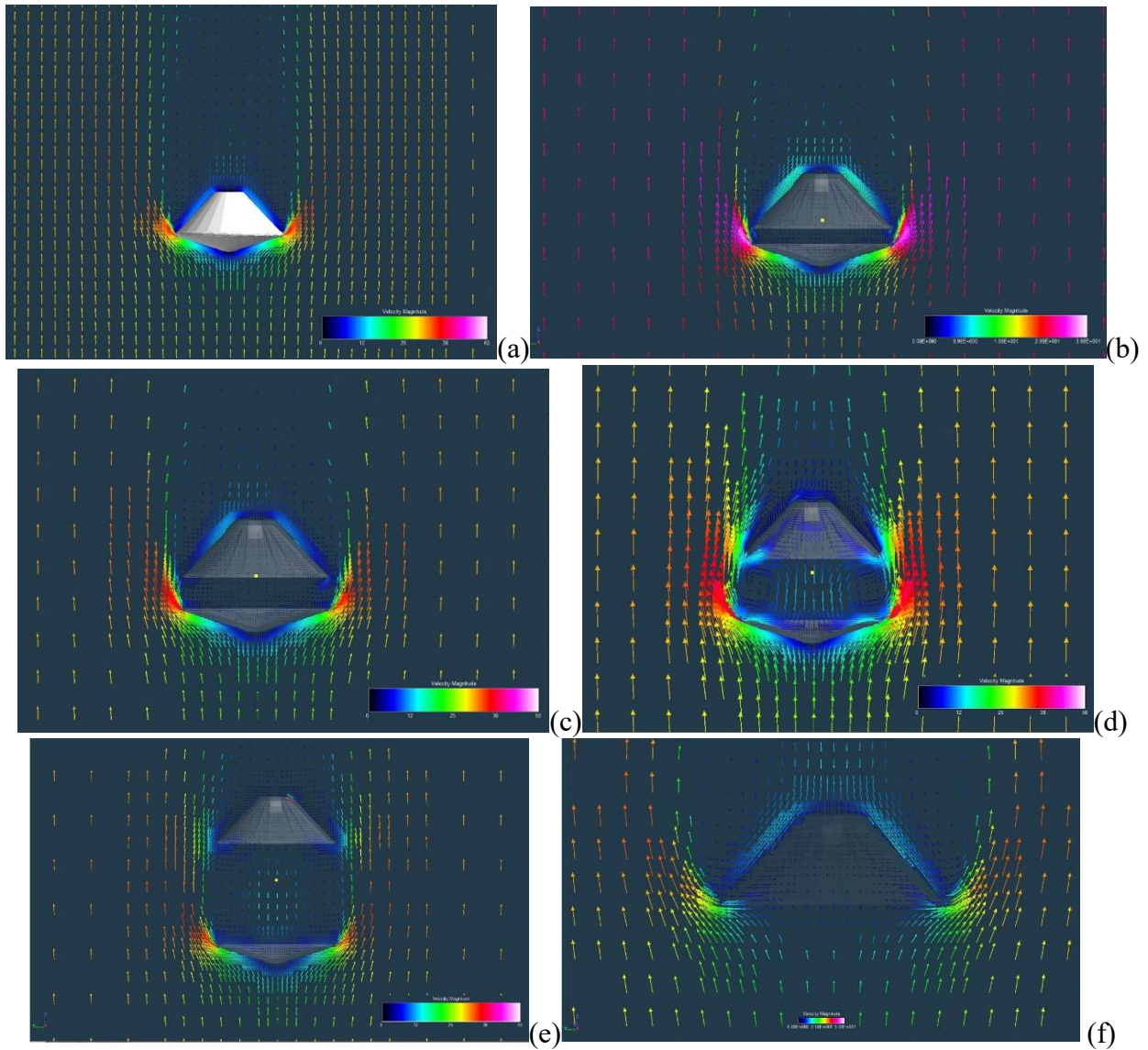
Figure 8.   Heat shield "drop' from back shell (no payload contents, i.e. hollow cavity): (a) Separation of z/D=0; (b) z/D=0.1; (c) z/D=0.2; (d) z/D=0.4; (e) z/D=0.8; (f) z/D=∞

Figures 9-10 are flow field predictions showing rotors spinning pre- and post-release (collective = 0 Deg.) and resulting rotor downwash (rotors only, i.e. no fuselage).
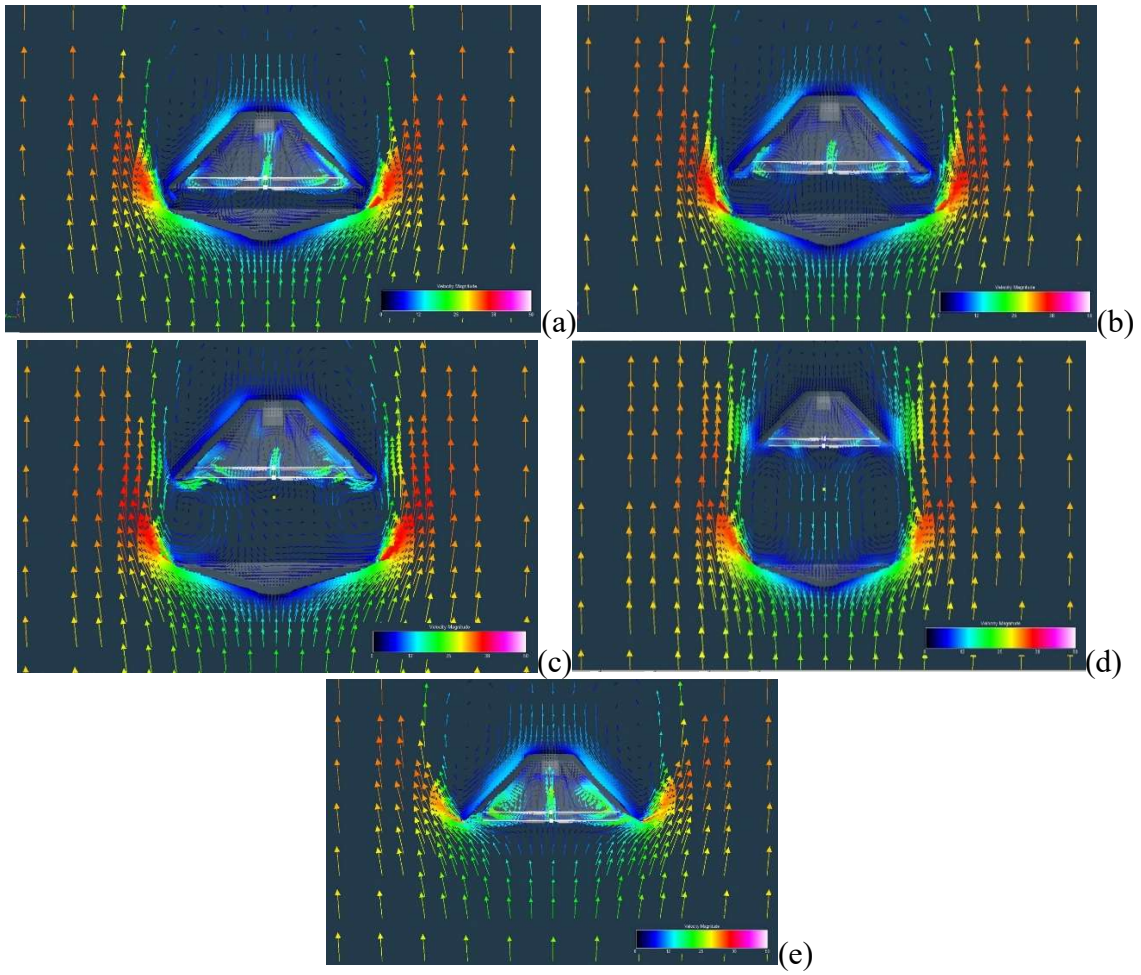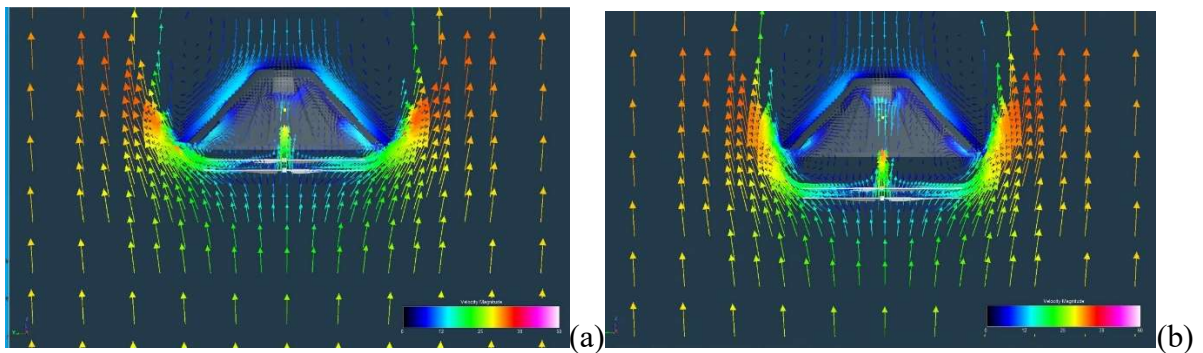
Figure 9. Rotor spin-up (attached to back shell) as heat shield separates (collective = 0 Deg.): (a) separation of z/D=0.1; (b) z/D=0.2; (c) z/D=0.4; (d) z=0.8; (e) z/D=∞
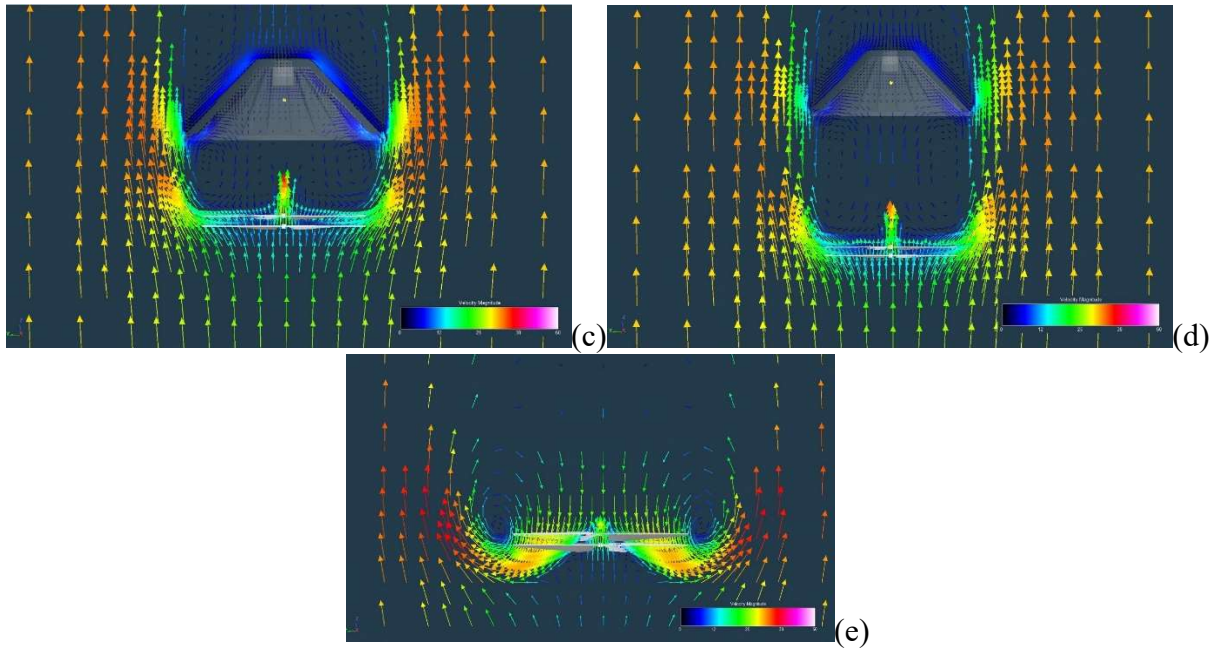
Figure 10.   Rotor downwash as coaxial rotors are released from the back shell (collective = 0 Deg.): (a) separation of z/D=0.1; (b) z/D=0.2; (c) z/D=0.4; (d) z=0.8; (e) z/D=∞

Potential Use of Negative Thrust to Augment Deployment of MHH from Back Shell

A major consideration is how to ensure that the Mars Highland Helicopter deploys safely from the back shell. In an ideal sense, the relative ballistic coefficients of the parachute and back shell are lower than the ballistic coefficient of the powered 'free-falling' MHH.   That may or may not be possible. Alternately, it might be possible to reduce collective to negative blade pitch angles so that negative thrust is generated. The rotor blades are twisted with -10 degrees linear twist. The negative thrust cases were run at collectives of -5 Deg.   The negative thrust would help safely propel the aerial vehicle from the back shell.   Negative thrust will have implications for the rotor control system as well as the drive train mechanical design (e.g. different bearing types/arrangements). Figure 11 presents flow predictions of rotors at negative thrust within the sealed aeroshell.
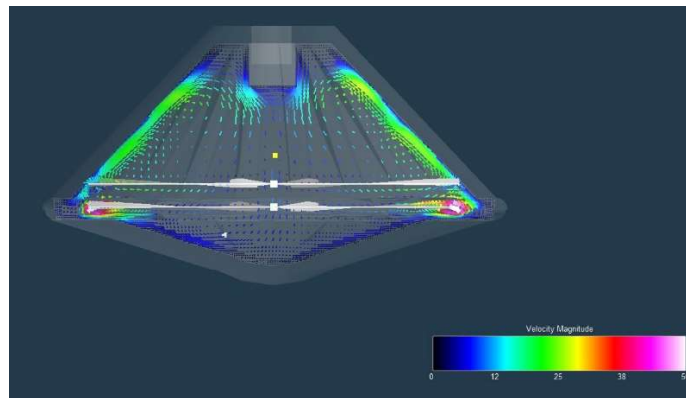

Figure 11. Rotors operating at negative thrust in the sealed aeroshell (collective = -5Deg.)

12

Figure 12 examines the rotor downwash as the vehicle descends with assistance from negative thrust from the rotors.
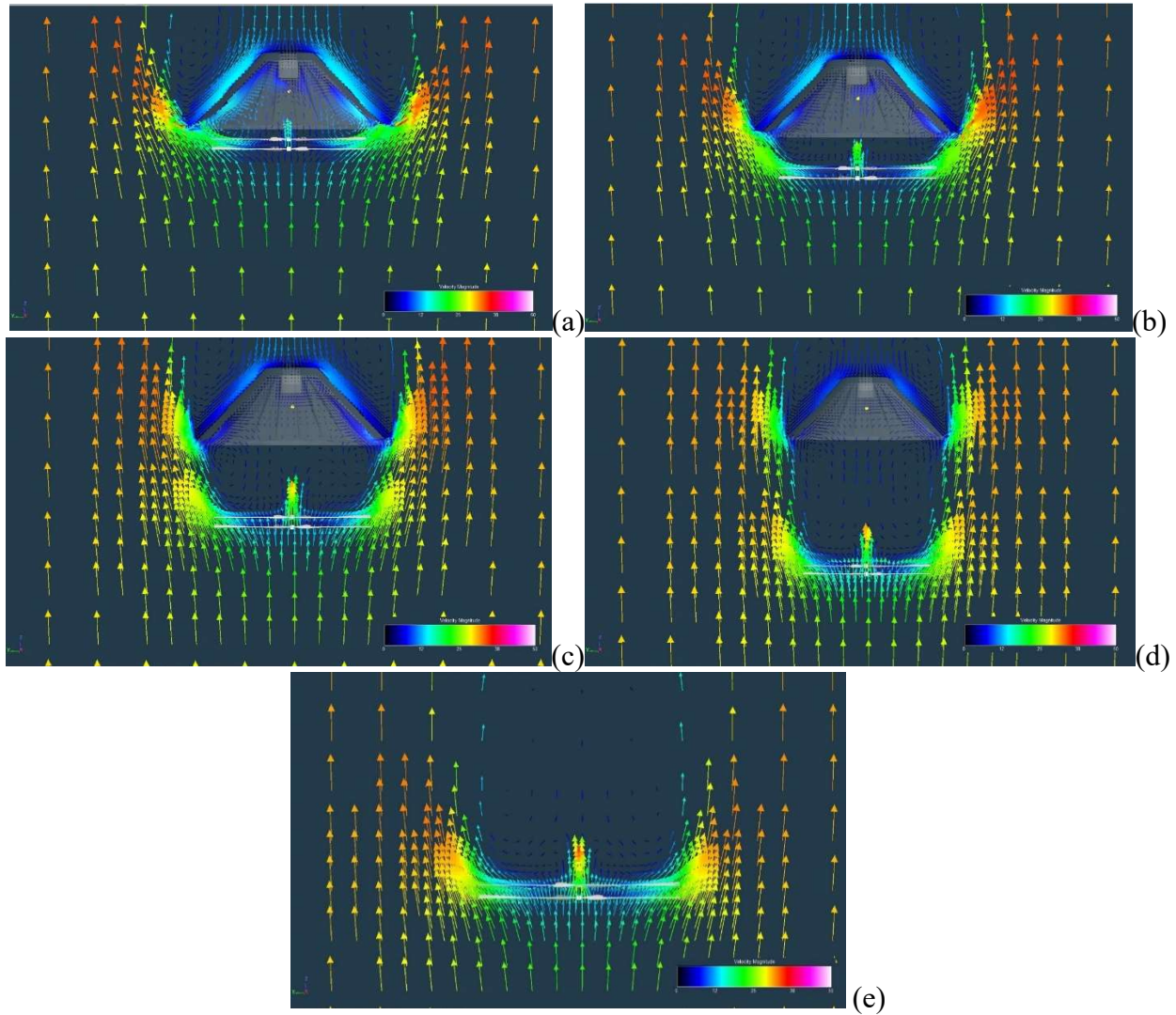

Figure 12. Rotor downwash as coaxial configuration separates from back shell (collective = -5 Deg.): (a) separation of z/D=0.1; (b) z/D=0.2; (c) z/D=0.4; (d) z=0.8; (e) z/D=∞

Mid-Air-Deployment Powered Descent Profiles

Quasi-Steady CFD Predictions of Descent (rotors only)

Figures 13 and 14 expand upon the earlier CFD predictions for rotors-only post-release from the EDL backshell. Figures 10 and 12 were for collectives of 0 and -5 Deg. Figures 13 and 14 are for collectives of 5 and 10 Deg, These results are only a subset of overall collective cases run.
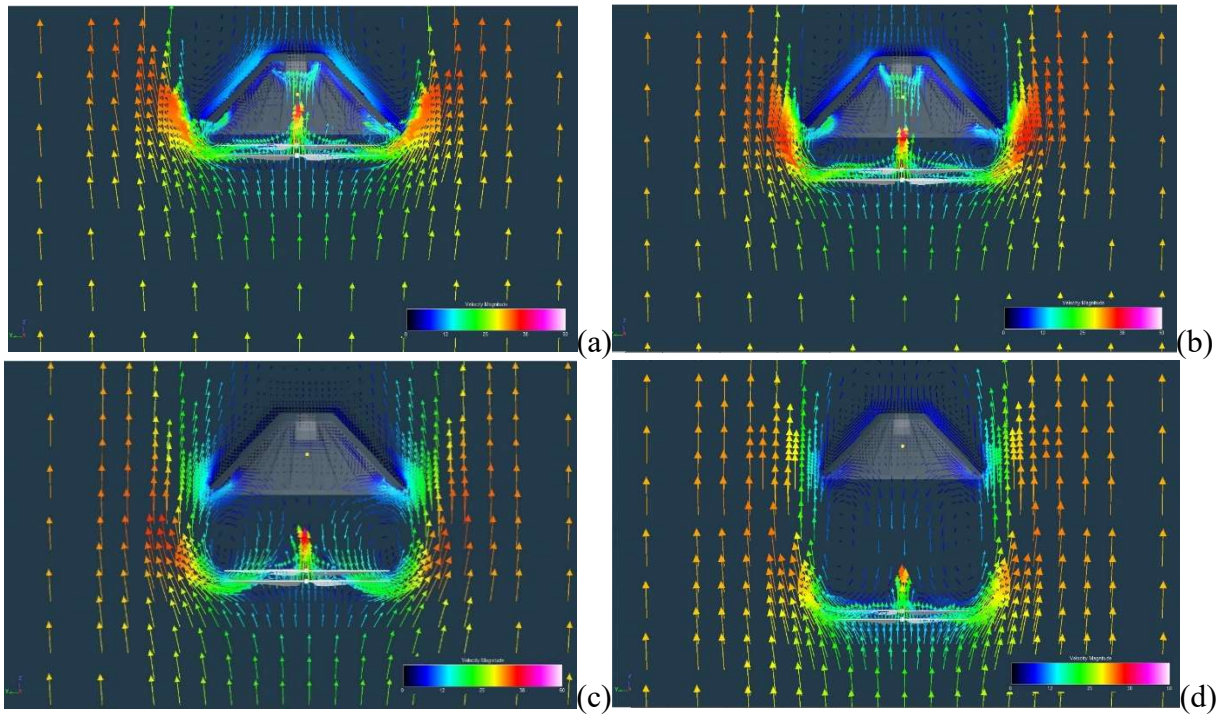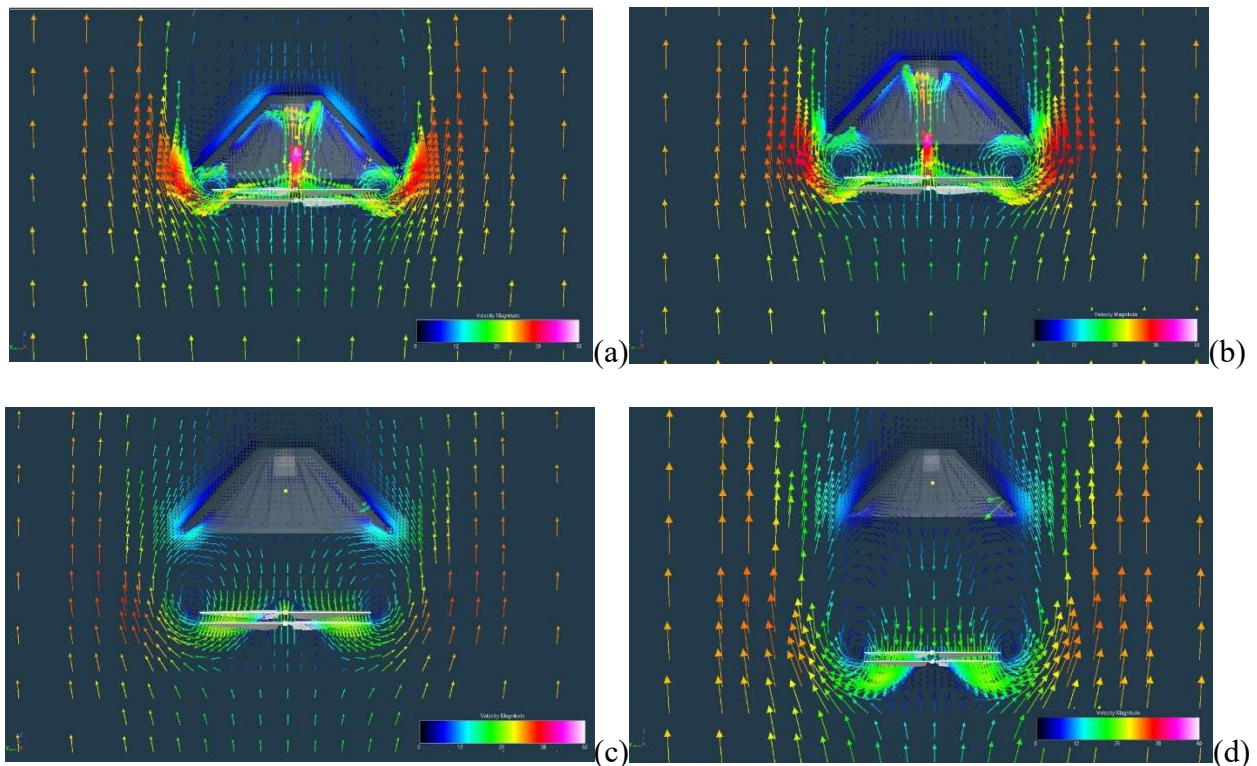
Figure 13. Initial MHH 'drop,' or release, from back shell (both rotors are at collective = 5 Deg.): (a) z_{rotor}/D=0.1; **(b)** z_{rotor}/D=0.2; **(c)** z_{rotor}/D=0.4; **(d)** z_{rotor}/D=0.8

Figure 14. Initial MHH 'drop,' or release, from back shell (both rotors are at collective = 10 Deg.): (a) z_{rotor}/D=0.1; **(b)** z_{rotor}/D=0.2; **(c)** z_{rotor}/D=0.4; **(d)** z_{rotor}/D=0.8

Figure 15 illustrates the influence of descent speed on the rotor flow field (after the release and the MHH has fallen some distance) for a collective of 10 Deg. at a shaft angle of zero degrees (pure vertical descent). The formation and propagation of a descent vortex ring (as a part of entering vortex ring state and transitioning or approaching turbulent wake state) can be seen.
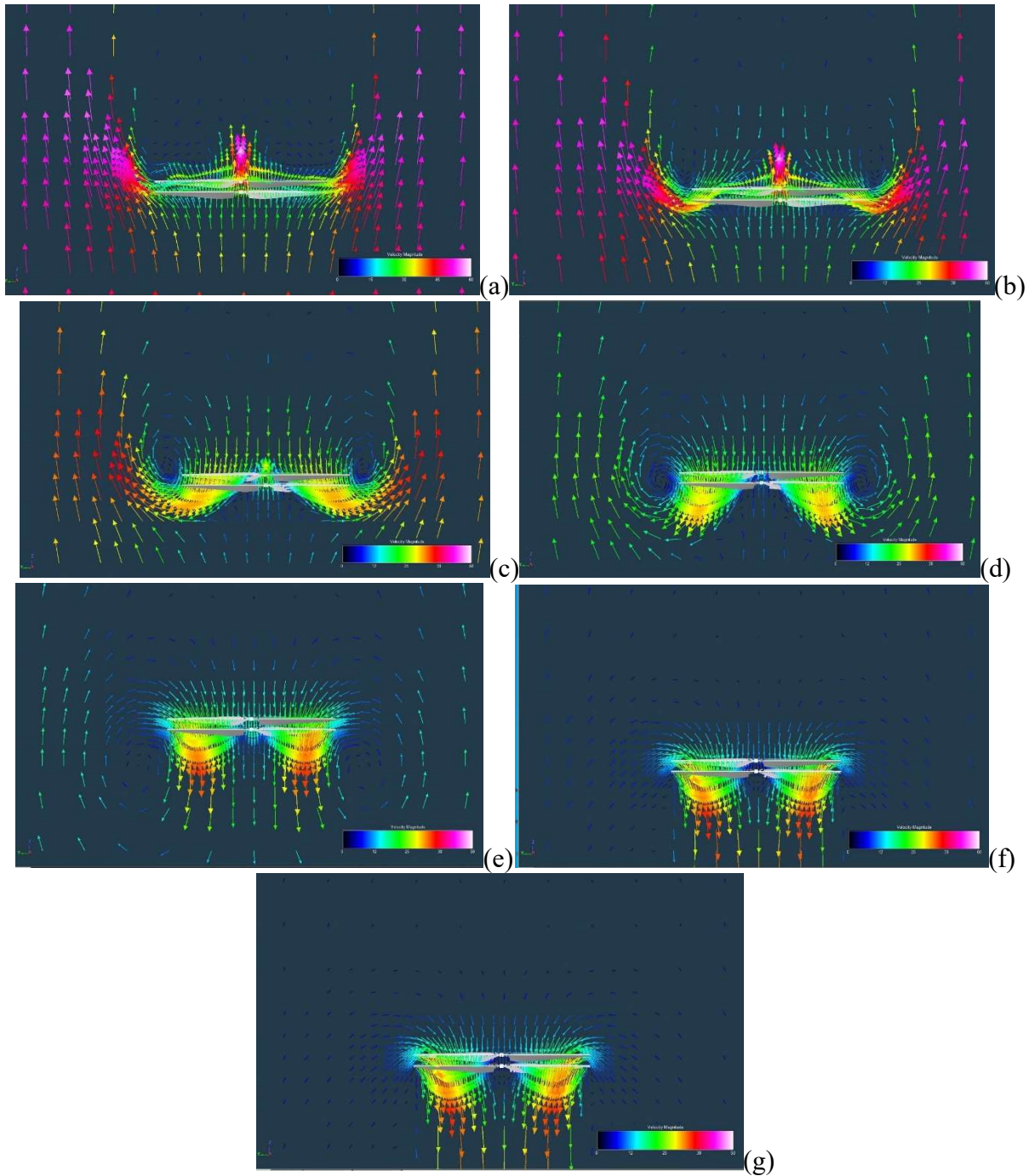

Figure 15. Flow field predictions for various descent rates (rotor shaft angle=0 Deg. and collective = 10 Deg.): (a) V_D=50m/s, (b) V_D=40m/s, (c) V_D=30m/s (initial release speed), (d) V_D=20m/s, (e) V_D=15m/s, (f) V_D=10m/s, and (g) V_D=5m/s

Figures 16 and 17 present the corresponding thrust and torque coefficients as a function of the MHH coaxial rotor collective and descent speed. Coaxial rotor performance in descent is more complex than that of a single-rotor descent. Both the thrust and torque coefficient trends are very nonlinear. Further, the upper rotor (now in the wake of lower rotor) was comparatively more affected by descent speed and rotor collective than the lower rotor. Additionally, it seems that the character of the rotor flow fields and the thrust and torque trends abruptly change at a descent speed of ~15 m/s (V_D/V_{Tip} = ~0.08).
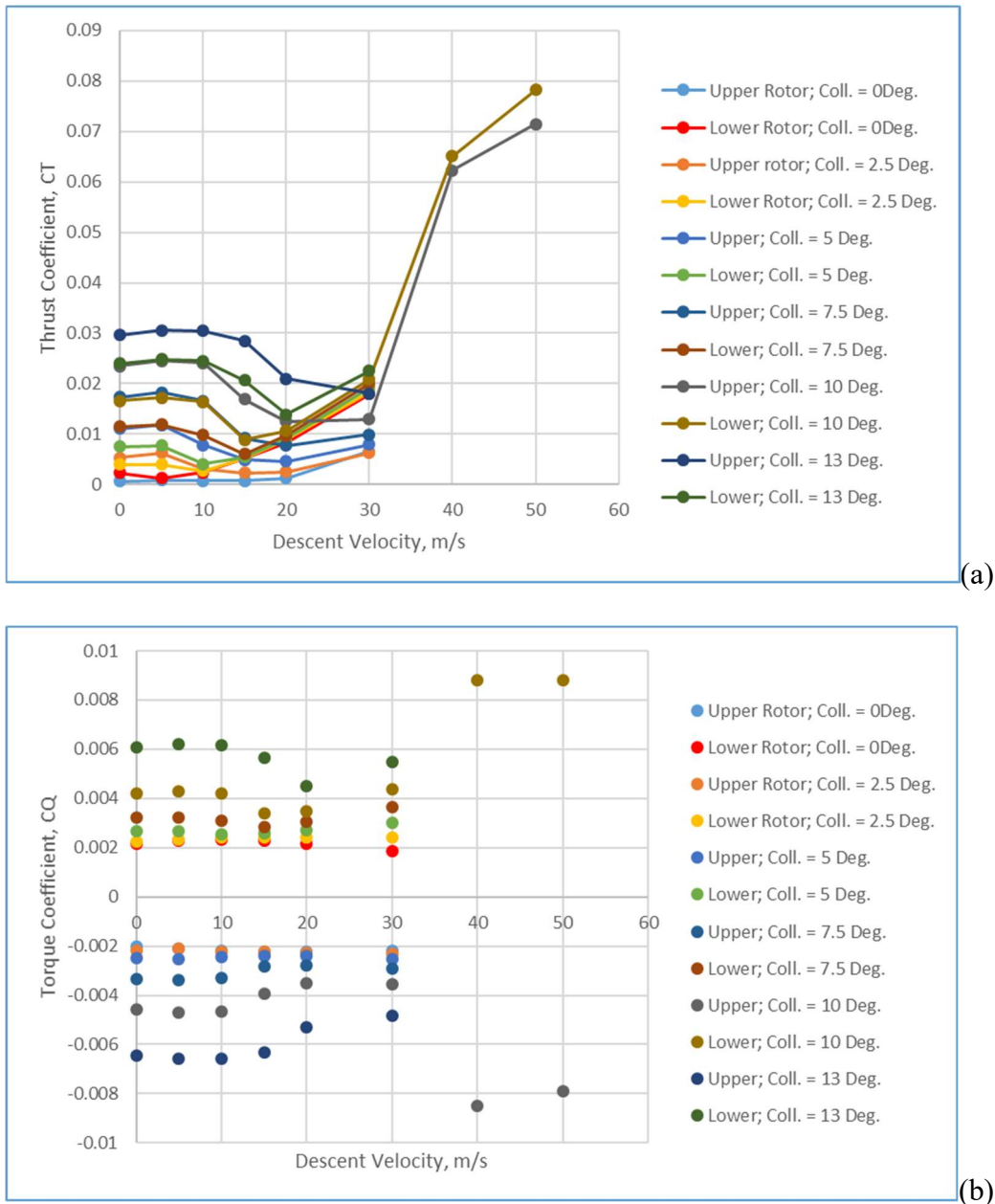

(a)

(b)

Figure 16. Thrust and torque coefficient trends with descent velocity for various collectives
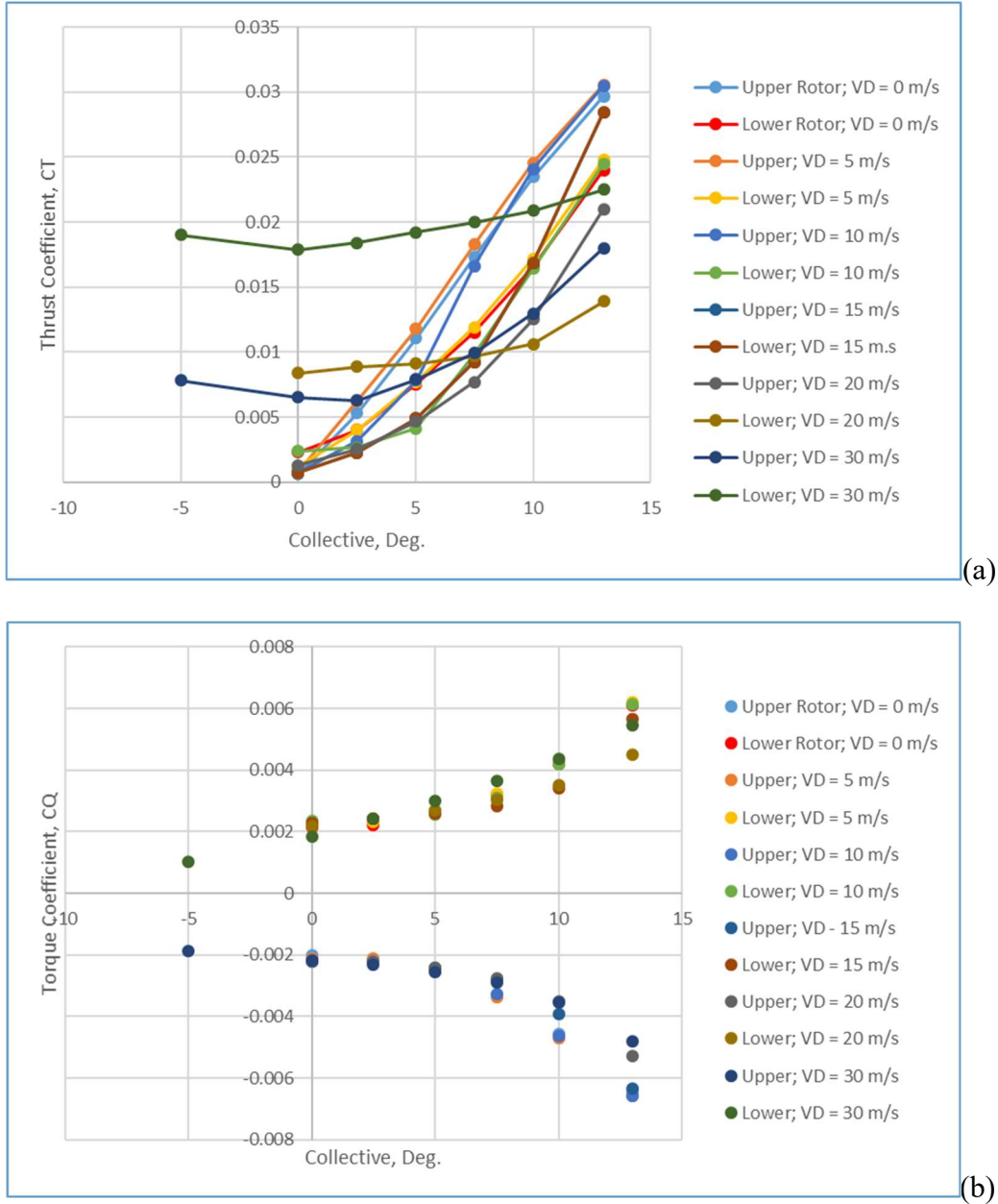
16

(a)

(b)

Figure 17. Rotor (upper and lower) torque coefficients (C_Q) and thrust coefficients (C_T): (a) C_T as a function of collective and (b) C_Q as a function of collective

Figures 18-19 illustrate the influence of rotor shaft angle on the flow field for various descent speeds. Both rotors are at the same collective (at ten degrees and, so, coaxial rotors are not torque-balanced) without cyclic control input for trimming (the rotor blades are at fixed pitch). Keeping the rotors at a fixed collective, without cyclic trim or torque-balancing, considerably simplifies

this initial modeling and is appropriate for this initial Mars Highland Helicopter mid-air-deployment study.
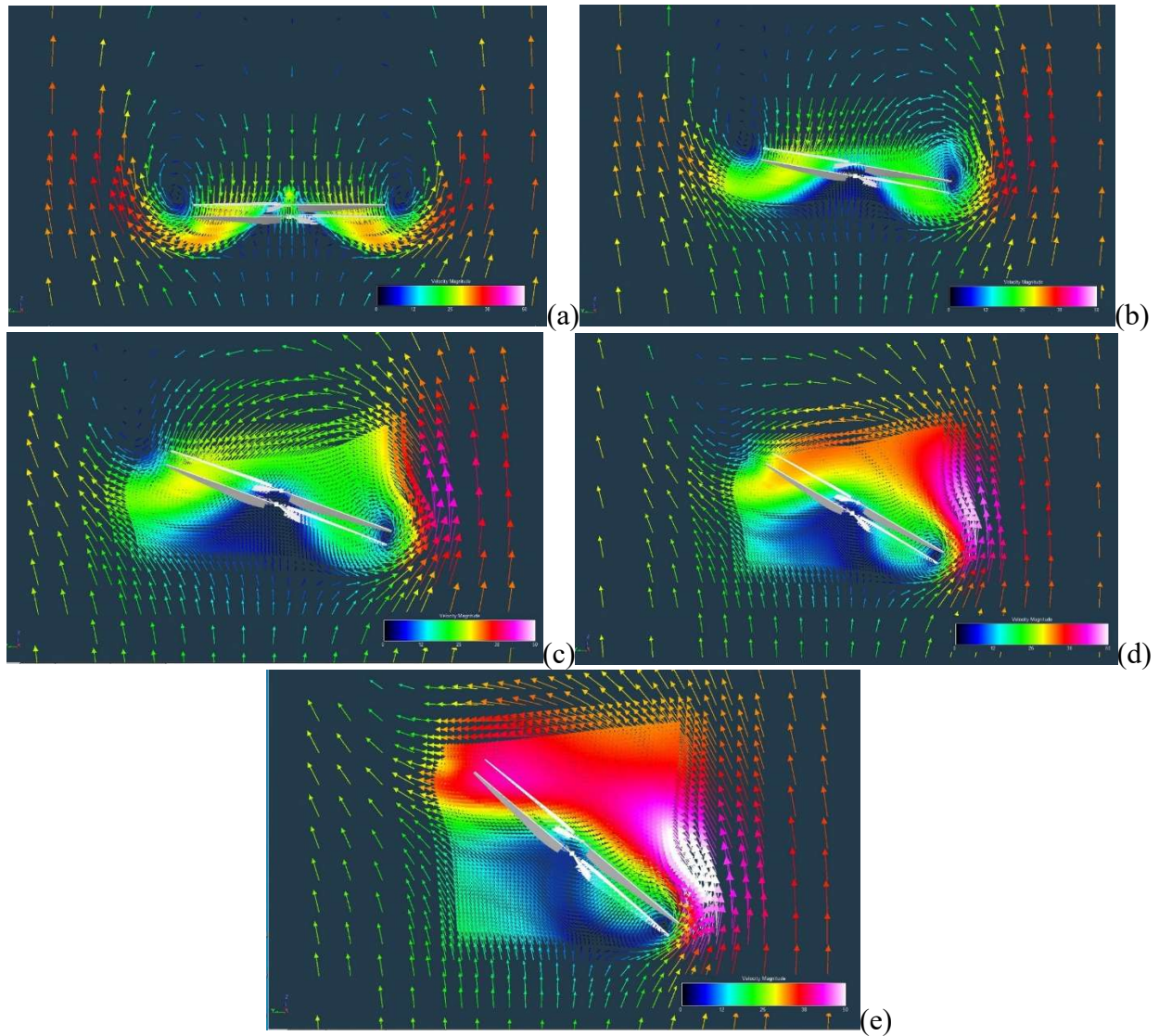

Figure 18. Rotor shaft angle sweep (V_D=30m/s and collectives = 10Deg.): (a) α_s=0Deg., (b) α_s=10Deg., (c) α_s=20Deg., (d) α_s=30Deg., and (e) α_s=40Deg.

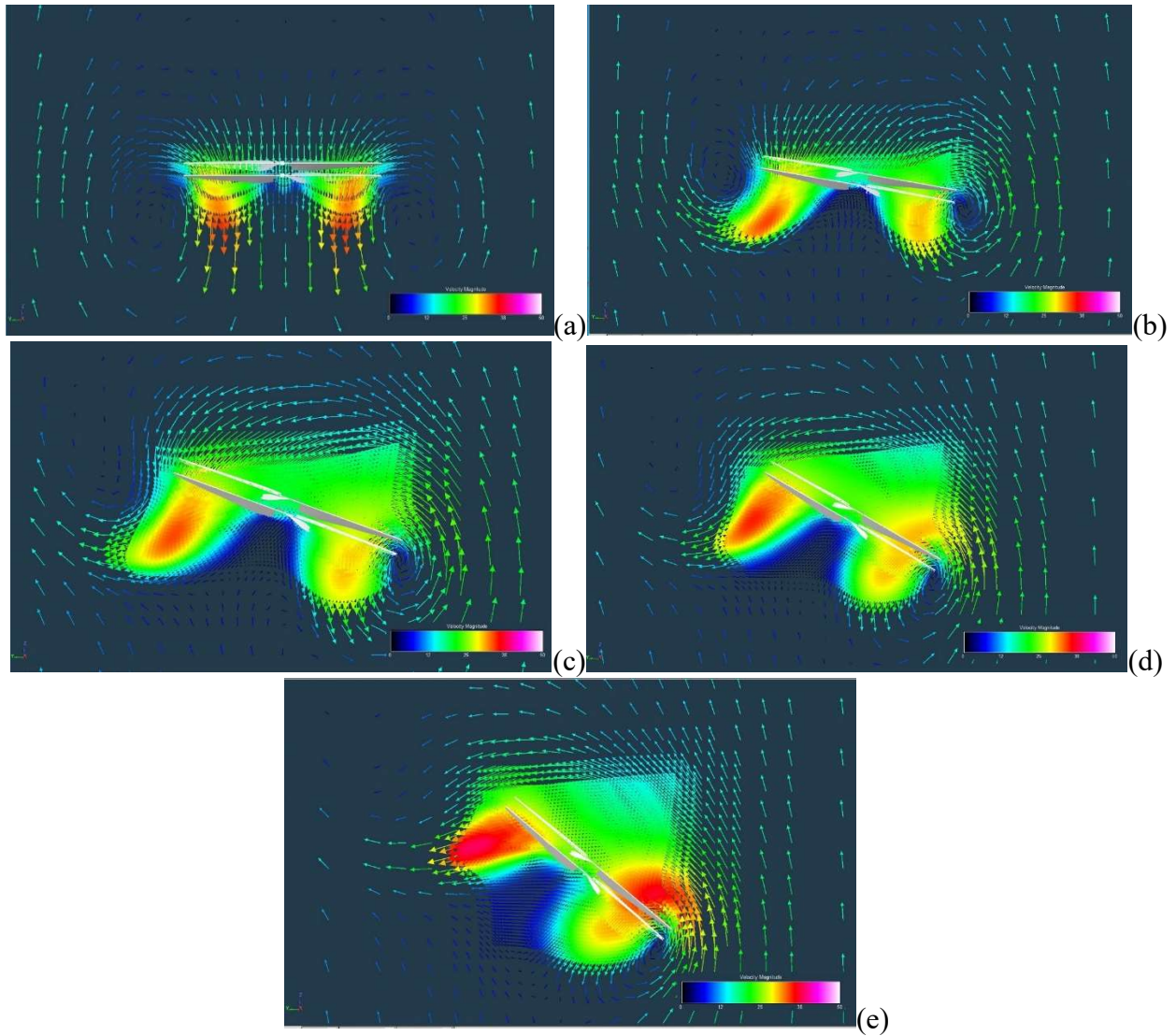Figure 19a-e presents the flow field predictions for a descent speed of 15m/s for various rotor shaft angles.

Figure 19. Rotor shaft angle sweep (V_D=15m/s and collectives = 10Deg.): (a) α_s=0Deg., (b) α_s=10Deg., (c) α_s=20Deg., (d) α_s=30Deg., and (e) α_s=40Deg.

Figure 20 presents the predicted influence of rotor shaft angle (vehicle attitude) on rotor thrust and torque coefficients. It is necessary during the initial phase of the MHH descent profile to command small nosedown attitudes to move the vehicle laterally away from the path of the falling aeroshell and parachute to avoid possible collision. However, this reduces the amount of vertical deceleration possible and, so, these two competing requirements need to be traded off against each other.
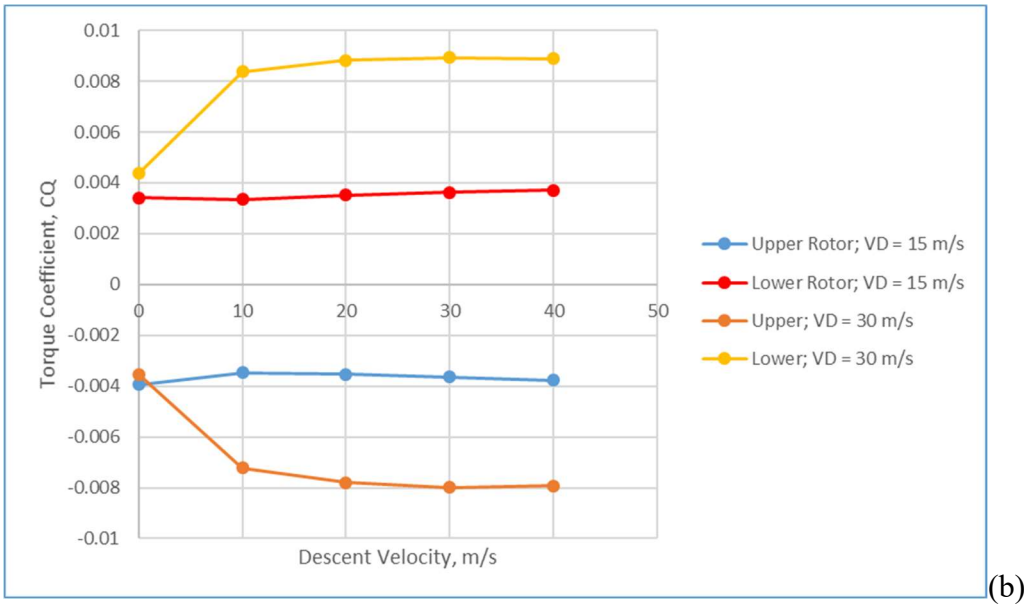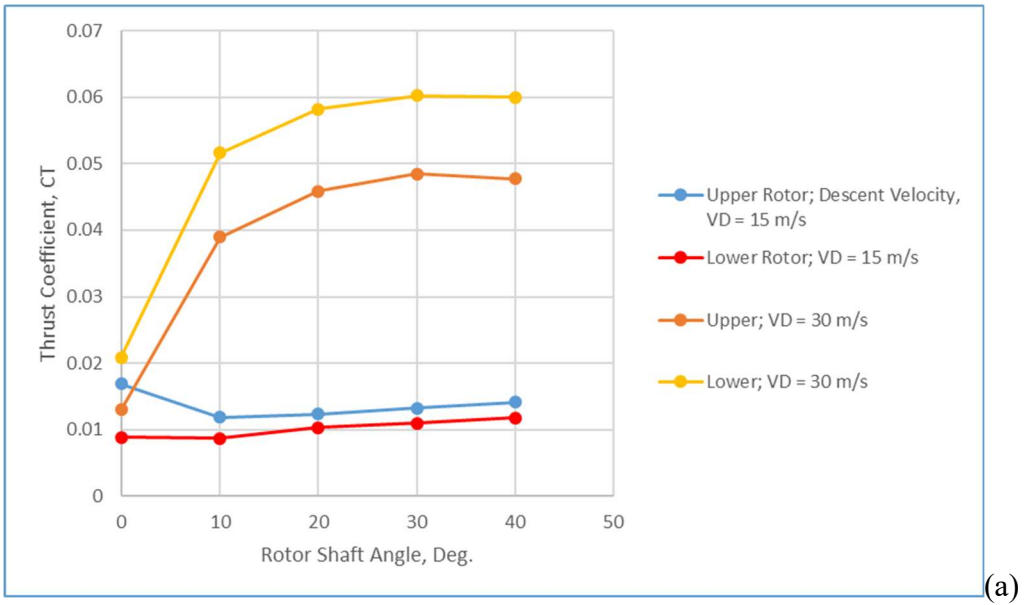
(a)

(b)

Figure 20. Thrust and torque coefficients as a function of rotor shaft angle at two different descent speeds

Quasi-Steady CFD Predictions of Descent (with fuselage)

Figure 21a-b presents predicted flow field results for descent, in the earliest stages of release from the aeroshell, for not just rotors-only but also incorporating a notional MHH fuselage design. As can be seen in these flow field results, there is more asymmetry being predicted in the backshell wake than as compared to the quasi-steady rotors-only results shown earlier in the paper. It would seem, at first, that the flow should be relatively axisymmetric but, in reality, bluff body separated flow tends to have asymmetric shifts in their wakes and therefore the flow is fully three-dimensional and unsteady (things shift around with time).   This asymmetry may result in some level of backshell 'wobble' during MHH release. Clearly these results will have to be looked at in depth in follow-on work for the MHH project. Sometimes, experimentally, trips, trip wires, and small vortex generators are used to help stabilize the flow and keep bluff body wakes from shifting around too much. Unfortunately, model trips and VG's is likely beyond the capability of a mid-fidelity tool like RotCFD. Note that no solar array is modeled above the rotors in a rotor-mast-mounted configuration.   This will be added in later CFD predictions.
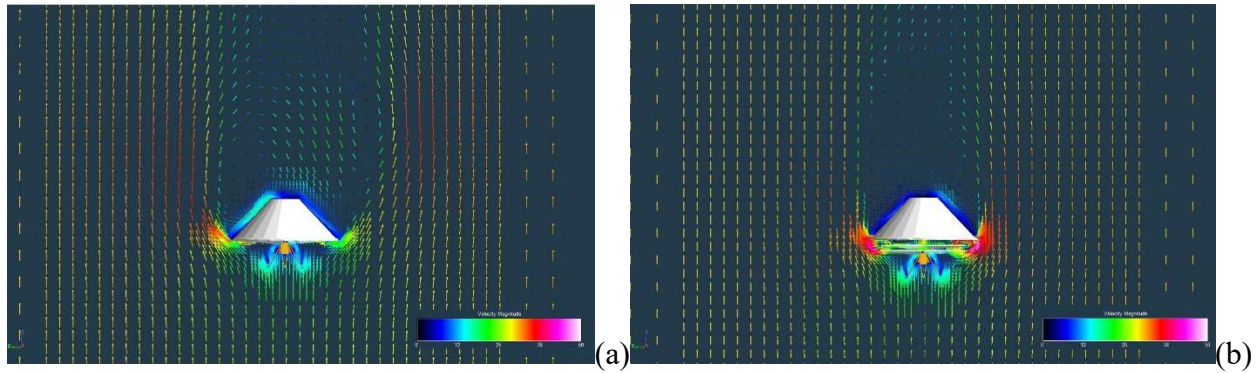

(a)   (b)

Figure 21. Predicted flow fields for MHH with fuselage: (a) $z_{rotor}/D = 0$ and (b) $z_{rotor}/D = 0.1$

Powered Descent Profiles as Determined from Surrogate Model derived from CFD Results

There is a moderate body of past work in the literature examining autorotation and (partial) powered descent of rotary wing, e.g. Ref. 11.   Among this work are studies into rotary-wing autorotation/descent for entry/reentry space exploration applications, e.g. Ref. 12. Many of these studies used classic analytical rotary-wing modeling extended/tailored to the entry/reentry descent problem.   Beyond analytical and CFD modeling, there is a small but important body of experimental work, for example, Refs. 15-17. Future Mars Highland Helicopter work will also experimentally examine mid-air-deployment issues.

A surrogate model is derived from the rotors-only in free descent RotCFD predictions as summarized as in Figs. 16, 17, and 20. This surrogate model is summarized in Eqs. 1-5.

$$F_z = (C_{TU}A_U V_{TU}^2 + C_{TL}A_L V_{TU}^2)\rho cos\alpha_{shaft}$$

$$F_x = (C_{TU}A_U V_{TU}^2 + C_{TL}A_L V_{TU}^2)\rho \sin\alpha_{shaft}$$

$$P = (C_{PU}A_U V_{TU}^3 + C_{PL}A_L V_{TU}^3)\rho$$

$$C_{PU} = |C_{QU}| \qquad C_{PL} = |C_{QL}|$$

<div align="right">(1a-e)</div>

From regression analysis of the RotCFD results, the following expressions were derived, Eqs. 2-4. This surrogate model is limited to two rotor collective settings, 10 and 13 Deg., (assumed to be applied to both rotors, i.e. the rotors are not torque-balanced in this initial first-order analysis). These collective settings are relatively low to reflect collective physical limitations for the closely-spaced (rotor-to-rotor separation) coaxial rotors required for stowing the 2m diameter rotors in the Pathfinder-type EDL aeroshell.

For the upper rotor:

$$C_{TU} = (a_{0U} + a_{1U}V_D + a_{2U}V_D^2 + a_{3U}V_D^3 + a_{4U}V_D^4)(c_{0U} + c_{1U}\alpha_{shaft} + c_{2U}\alpha_{shaft}^2 + c_{3U}\alpha_{shaft}^3)$$

$$C_{QU} = (b_{0U} + b_{1U}V_D + b_{2U}V_D^2)(d_{0U} + d_{1U}\alpha_{shaft} + d_{2U}\alpha_{shaft}^2 + d_{3U}\alpha_{sha}^3 \ )$$

$$a_{0U} = \begin{cases} 0.0211 & \theta_{0.75} = 10 \\ 0.0292 & \theta_{0.75} = 13 \end{cases} \qquad a_{1U} = \begin{cases} 3.97 \cdot 10^{-3} & \theta_{0.75} = 10 \\ 1.01 \cdot 10^{-3} & \theta_{0.75} = 13 \end{cases}$$

$$a_{2U} = \begin{cases} -5.46 \cdot 10^{-4} & \theta_{0.75} = 10 \\ -1.10 \cdot 10^{-4} & \theta_{0.75} = 13 \end{cases} \qquad a_{3U} = \begin{cases} 1.97 \cdot 10^{-5} & \theta_{0.75} = 10 \\ 2.12 \cdot 10^{-6} & \theta_{0.75} = 13 \end{cases}$$

$$a_{4U} = \begin{cases} -2.00 \cdot 10^{-7} & \theta_{0.75} = 10 \\ 0 & \theta_{0.75} = 13 \end{cases}$$

$$c_{0U} = \begin{cases} 1 & V_D < 15 \\ 0.9962 + 0.0189\left(\dfrac{V_D}{15} - 1\right) & 15 \le V_D \le 30 \\ 1.0151 & V_D > 30 \end{cases}$$

$$c_{1U} = \begin{cases} 0 & V_D < 15 \\ -0.0465 + 0.3218\left(\dfrac{V_D}{15} - 1\right) & 15 \le V_D \le 30 \\ 0.2753 & V_D > 30 \end{cases}$$

$$c_{2U} = \begin{cases} 0 & V_D < 15 \\ 0.0021 - 0.0114\left(\dfrac{V_D}{15} - 1\right) & 15 \le V_D \le 30 \\ -0.0093 & V_D > 30 \end{cases}$$

$$c_{3U} = \begin{cases} 0 & V_D < 15 \\ -3 \cdot 10^{-5} + 1.3 \cdot 10^{-4}\left(\dfrac{V_D}{15} - 1\right) & 15 \le V_D \le 30 \\ 1.0 \cdot 10^{-4} & V_D > 30 \end{cases}$$

$$b_{0U} = \begin{cases} -4.86 \cdot 10^{-3} & \theta_{0.75} = 10 \\ -6.57 \cdot 10^{-3} & \theta_{0.75} = 13 \end{cases} \qquad b_{1U} = \begin{cases} 1.17 \cdot 10^{-4} & \theta_{0.75} = 10 \\ -2.24 \cdot 10^{-6} & \theta_{0.75} = 13 \end{cases}$$

$$b_{2U} = \begin{cases} -3.87 \cdot 10^{-6} & \theta_{0.75} = 10 \\ 2.16 \cdot 10^{-6} & \theta_{0.75} = 13 \end{cases}$$

$$d_{0U} = \begin{cases} 1 & V_D < 15 \\ 0.9986 + 0.0118\left(\dfrac{V_D}{15} - 1\right) & 15 \le V_D \le 30 \\ 1.0104 & V_D > 30 \end{cases}$$

$$d_{1U} = \begin{cases} 0 & V_D < 15 \\ -0.0185 + 0.1663\left(\dfrac{V_D}{15} - 1\right) & 15 \le V_D \le 30 \\ 0.1478 & V_D > 30 \end{cases}$$

$$d_{2U} = \begin{cases} 0 & V_D < 15 \\ 0.0009 - 0.0065\left(\dfrac{V_D}{15} - 1\right) & 15 \le V_D \le 30 \\ -0.0056 & V_D > 30 \end{cases}$$

$$d_{3U} = \begin{cases} 0 & V_D < 15 \\ -1 \cdot 10^{-5} + 8 \cdot 10^{-5}\left(\dfrac{V_D}{15} - 1\right) & 15 \le V_D \le 30 \\ 7 \cdot 10^{-5} & V_D > 30 \end{cases}$$

For the lower rotor:

$$C_{TL} = \left(a_{0L} + a_{1L}V_D + a_{2L}V_D^2 + a_{3L}V_D^3 + a_{4L}V_D^4\right)\left(c_{0L} + c_{1L}\alpha_{shaft} + c_{2L}\alpha_{shaft}^2 + c_{3L}\alpha_{shaft}^3\right)$$

$$C_{QL} = \left(b_{0L} + b_{1L}V_D + b_{2L}V_D^2\right)\left(d_{0L} + d_{1L}\alpha_{shaft} + d_{2L}\alpha_{shaft}^2 + d_{3L}\alpha_{shaft}^3\right)$$

$$a_{0L} = \begin{cases} 0.0154 & \theta_{0.75} = 10 \\ 0.0234 & \theta_{0.75} = 13 \end{cases} \qquad a_{1L} = \begin{cases} 2.47 \cdot 10^{-3} & \theta_{0.75} = 10 \\ 1.33 \cdot 10^{-3} & \theta_{0.75} = 13 \end{cases}$$

$$a_{2L} = \begin{cases} -3.83 \cdot 10^{-4} & \theta_{0.75} = 10 \\ -1.70 \cdot 10^{-4} & \theta_{0.75} = 13 \end{cases} \qquad a_{3L} = \begin{cases} 1.52 \cdot 10^{-5} & \theta_{0.75} = 10 \\ 4.14 \cdot 10^{-6} & \theta_{0.75} = 13 \end{cases}$$

$$a_{4L} = \begin{cases} -1.60 \cdot 10^{-7} & \theta_{0.75} = 10 \\ 0 & \theta_{0.75} = 13 \end{cases}$$

$$c_{0L} = \begin{cases} 1 & V_D < 15 \\ 0.9942 + 0.0175\left(\dfrac{V_D}{15} - 1\right) & 15 \le V_D \le 30 \\ 1.0117 & V_D > 30 \end{cases}$$

$$c_{1L} = \begin{cases} 0 & V_D < 15 \\ -0.0074 + 0.2148\left(\dfrac{V_D}{15} - 1\right) & 15 \le V_D \le 30 \\ 0.2074 & V_D > 30 \end{cases}$$

$$c_{2L} = \begin{cases} 0 & V_D < 15 \\ 0.001 - 0.0085\left(\dfrac{V_D}{15} - 1\right) & 15 \le V_D \le 30 \\ -0.0075 & V_D > 30 \end{cases}$$

$$c_{3L} = \begin{cases} 0 & V_D < 15 \\ -2 \cdot 10^{-5} + 1.1 \cdot 10^{-5}\left(\dfrac{V_D}{15} - 1\right) & 15 \le V_D \le 30 \\ 9 \cdot 10^{-5} & V_D > 30 \end{cases}$$

$$b_{0L} = \begin{cases} 0.00431 & \theta_{0.75} = 10 \\ 0.00640 & \theta_{0.75} = 13 \end{cases} \qquad b_{1L} = \begin{cases} -9.30 \cdot 10^{-5} & \theta_{0.75} = 10 \\ -8.64 \cdot 10^{-5} & \theta_{0.75} = 13 \end{cases}$$

$$b_{2L} = \begin{cases} 3.99 \cdot 10^{-6} & \theta_{0.75} = 10 \\ 1.57 \cdot 10^{-6} & \theta_{0.75} = 13 \end{cases}$$

$$d_{0L} = \begin{cases} 1 & V_D < 15 \\ 0.9983 + 0.0116\left(\dfrac{V_D}{15} - 1\right) & 15 \le V_D \le 30 \\ 1.0099 & V_D > 30 \end{cases}$$

$$d_{1L} = \begin{cases} 0 & V_D < 15 \\ -0.0048 + 0.1373\left(\dfrac{V_D}{15} - 1\right) & 15 \le V_D \le 30 \\ 0.1325 & V_D > 30 \end{cases}$$

$$d_{2L} = \begin{cases} 0 & V_D < 15 \\ 0.0004 - 0.0057\left(\dfrac{V_D}{15} - 1\right) & 15 \le V_D \le 30 \\ -0.0053 & V_D > 30 \end{cases}$$

$$d_{3L} = \begin{cases} 0 & V_D < 15 \\ -6 \cdot 10^{-6} + 6.6 \cdot 10^{-5}\left(\dfrac{V_D}{15} - 1\right) & 15 \le V_D \le 30 \\ 6 \cdot 10^{-5} & V_D > 30 \end{cases}$$

(3a-r)

Fuselage:

$$D_z = \frac{1}{2} f_{Az} \rho V_D^2$$

$$D_x = \frac{1}{2} f_{Ax} \rho V_x^2$$

$$f_{Az} \approx 0.04m^2$$

$$f_{Ax} \approx 1.6m^2$$

(4a-d)

Descent Equations of Motion:

$$m\ddot{h} = F_z + D_z - mg$$

$$m\ddot{x} = F_x - D_x$$

(5a-b)

The above equations (Eqs. 1-5) were solved with a Runge-Kutta ordinary differential equation solver. Note that in the above equations, the atmospheric density, ρ, and speed of sound, c, is a function of the vehicle alitude, h, Ref. 18. A range of vehicle masses and rotor collectives is prescribed in the below analysis. The goal is to release the vehicle at 5km altitude and reach zero descent velocity before or by 3.5km.
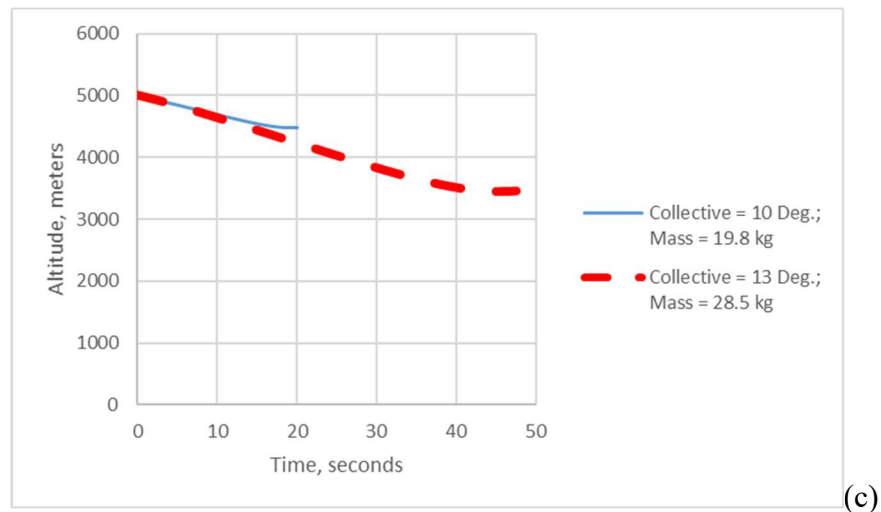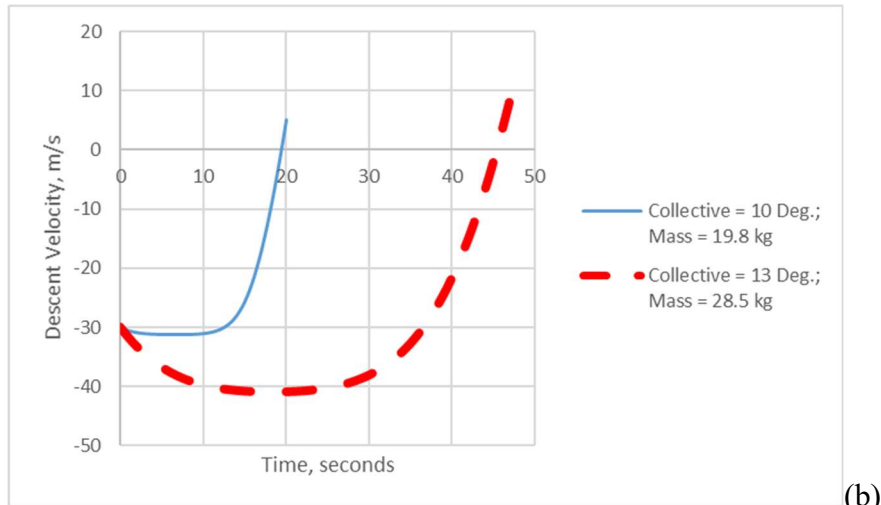

(a)

(b)

(c)
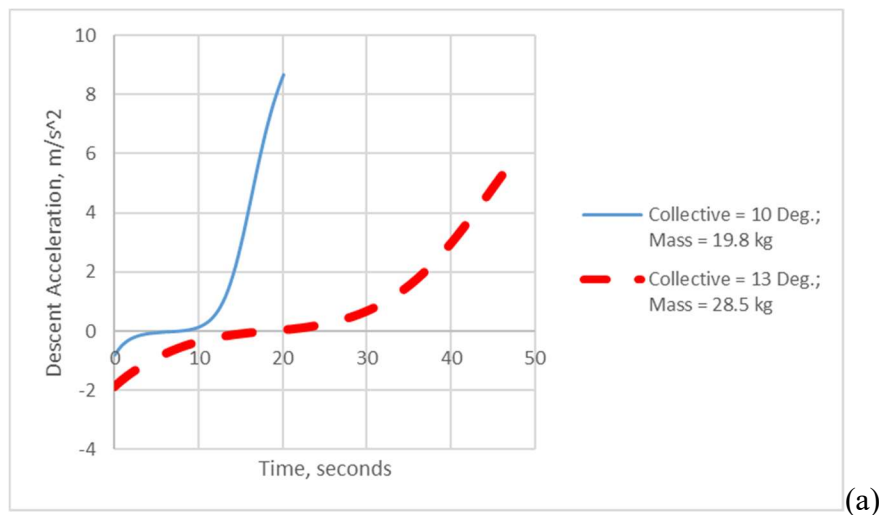
Figure 22. Descent profile (for a given vehicle mass and mean rotor collective; M_{Tip}=0.85): (a) descent accelerations; (b) descent velocities; (c) altitude profile

The effect of vehicle mass (for a fixed collective of 13 Deg.) on descent profile, i.e. altitude in meters, is presented in Fig. 22. The descent profiles seem to be two general types: a fast deceleration where descent is arrested after a few hundred meters and a slow deceleration where reaching the pullout design target of 3.5km (from an initial release from 5km) is barely possible. A modest vehicle mass increase of 10-15% (for a given nominal collective) can make the difference between fast and slow decelerations. Some fairly large margins will have to be built into the vehicle design between 1G thrust and max thrust to avoid irrecoverable descents due to winds, vehicle attitude adjustments, and other environmental factors. The initial results would also suggest a sensitivity of the vehicle mass, for a given collective/thrust, on whether a successful deceleration profile can be achieved or not. For example, for a collective of 10 Deg., increasing the vehicle mass from 19.8kg to 20kg resulted in going from a successful deceleration from 5km to 4.3km to a profile in which the vehicle descent cannot be arrested. In all cases presented, the rotor shaft angle is commanded nosedown to 5 Deg. from time after release (at 5km) of one second,

27

to restoring the shaft angle to zero degrees, at time equal to five seconds. If either the magnitude of shaft angle, or the time held at that shaft angle, are increased by a couple of degrees or seconds, then similarly the vehicle cannot be successfully decelerated.
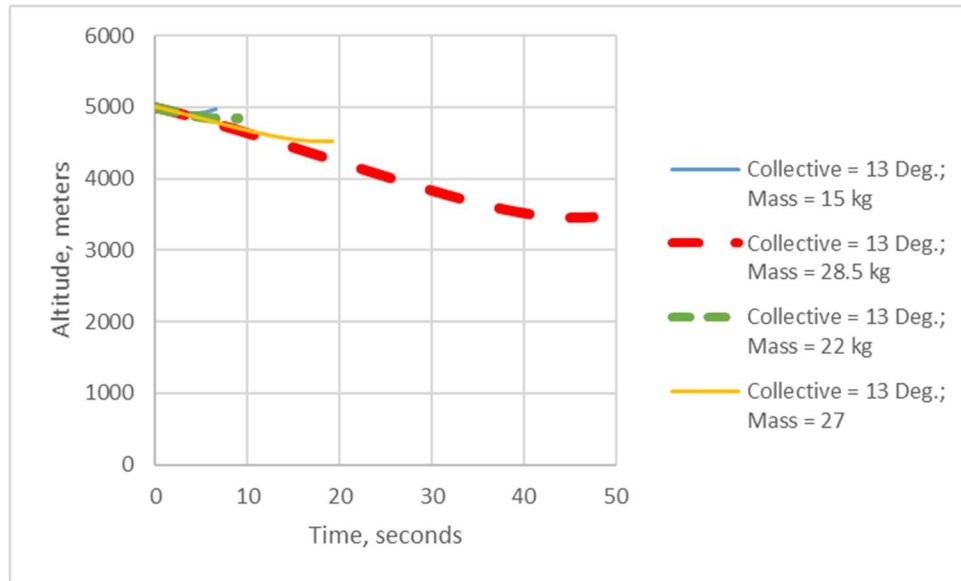

Figure 23. Descent (altitude) profiles for different vehicle masses for mean rotor collectives of 13 Deg. and M_{Tip}=0.85

As yet unexplored is how much winds could impact the vehicle descent profile. Substantial horizontal winds could result in significant reduction of deceleration capability of the rotors. These preliminary results, using the current form of the derived surrogate model, suggest that large margins need to be preserved in terms of rotor collective range and maximum thrust capability.

Energy and power management during MHH powered descent and pull-out to level flight (prior to initial VTOL landing) will be a key challenge. The descent/pull-out profile at an altitude of ~3.5-5km above the Martian highlands terrain will have profound implication as to battery sizing and overall power management strategies and electronics. The surrogate model developed for descent included torque and power coefficient expressions. These expressions can be used to make first-order estimates of rotor power during descent as well as being integrated to yield energy estimates.

Future work can take the first-order descent profile estimates stemming from surrogate models derived from quasi-steady CFD results and apply them to 'maneuvering' versions (rotors only) of RotCFD to look at unsteady aerodynamic effects of MHH descent.

Hover and Level Forward Flight in the Martian Highlands

A comparison of isolated rotor hover predictions from RotCFD and the well-known comprehensive rotorcraft aeromechanics analysis, CAMRAD II, softwre is presented in Fig. 24a-d. These hover predictions are for an early version model of a second-generation Mars Science

28

Helicopter (MSH), e.g. Ref. 3. The same airfoil tables (generated from a two-dimensional Navier-Stokes analysis performed for cambered circular-arc airfoils) are used for the RotCFD and CAMRAD II modeling. (A tip loss factor of 0.97 is used for the RotCFD modeling.) There is reasonable agreement between the two analyses in the mid-thrust and mid-collective ranges. Reasonable agreement at higher thrust levels was achievable only through tailored refined gridding on the RotCFD models (counter-intuitively reducing rotor refinement, as represented by the RRF=BxRF=4 (versus the rest of cases run at RRF=BxRF=9) designations, i.e. going for coarser grids). Yet unexplored is whether increased rotor refinement (even finer grids) would improve the agreement between the two analyses for the lower thrust and collective levels. This cross-validation has only been performed to date for isolated rotors under Mars-like conditions. Other RotCFD validation efforts for rotor performance for both terrestrial and Mars-like conditions can be seen in Refs. 8-9. This issue will continue to be explored.
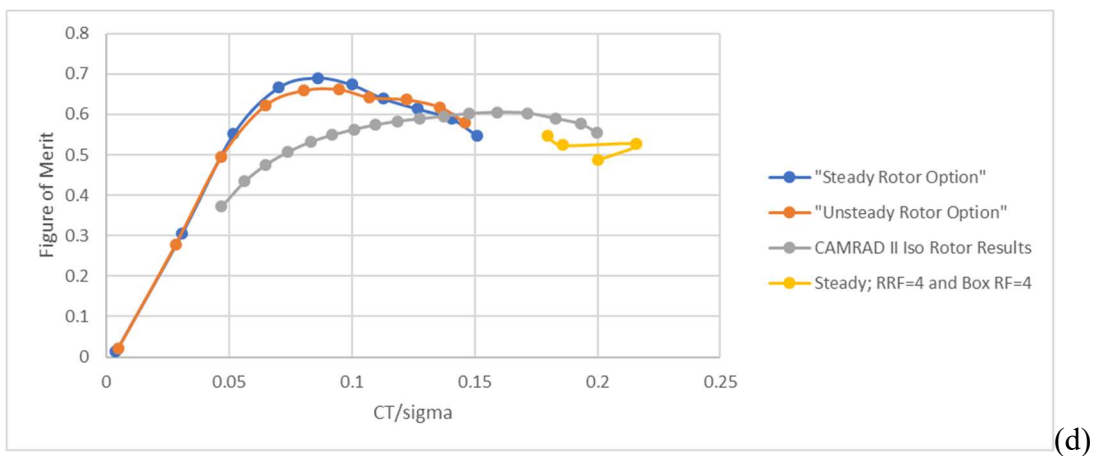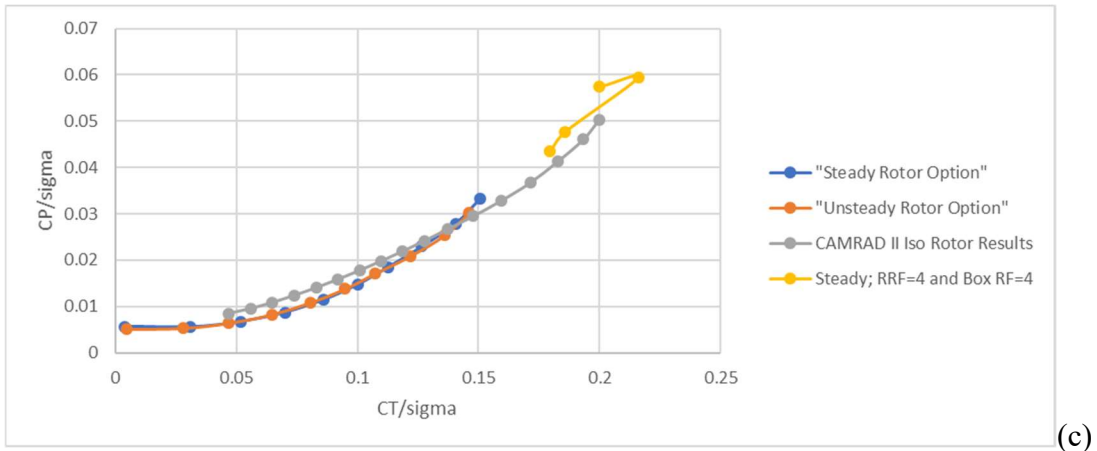

(a)

(b)

29

(c)

(d)
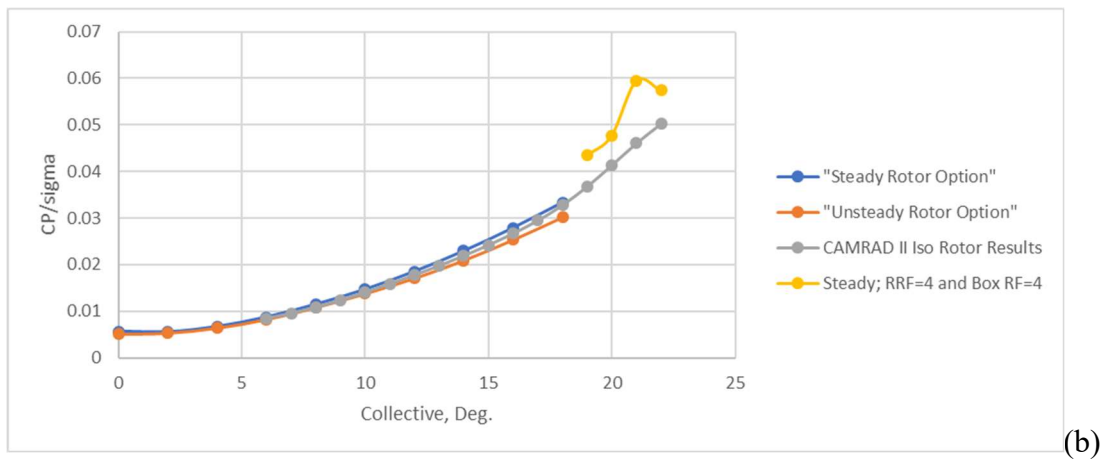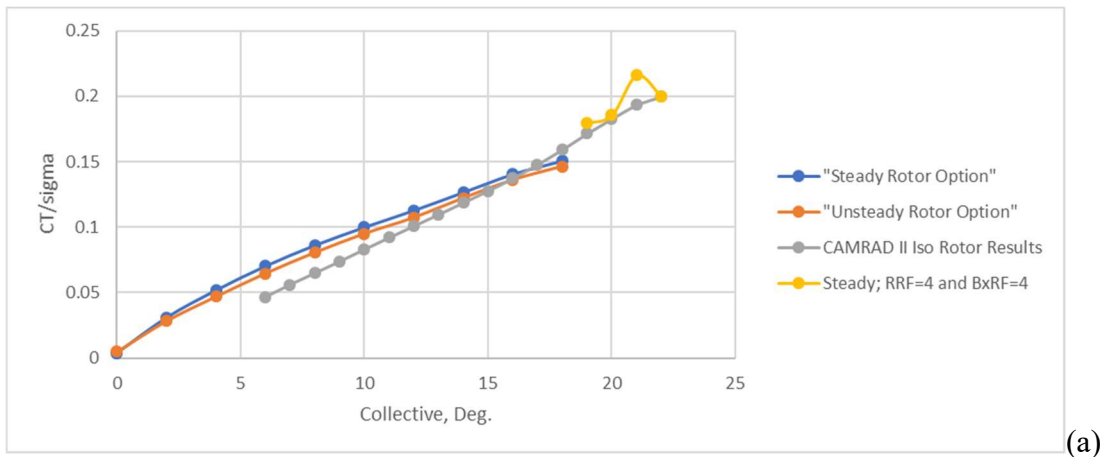
Figure 24. Rotor hover performance predictions for two different software tools: (a) CT/σ vs. collective; (b) CP/σ vs. collective; (c) CP/σ vs. CT/σ; (d) figure of merit vs. CT/σ

The key underpinning of the current work was the early establishing (through computational prediction) of the feasibility of VTOL flight in the Martian highlands. Aeroperformance and rotorcraft sizing tools used and validated during the Ingenuity Mars Helicopter Technology Demonstrator development were applied to this fundamental problem of establishing flight feasibility from a conceptual design perspective. All other technical challenges beyond this fundamental problem – including assessing the feasibility of mid-air-deployment of the rotorcraft – would have been moot if flight seemed unfeasible over the highlands.

Figures 25-26 show a 2m rotor diameter MHH in hover in ground effect and hover out of ground effect, with a notional fuselage and assuming a telescoping rotor mast so as to increase rotor-to-rotor spacing (and therefore greater collective and cyclic range) than the 'dropped,' or released, configuration as discussed previously.
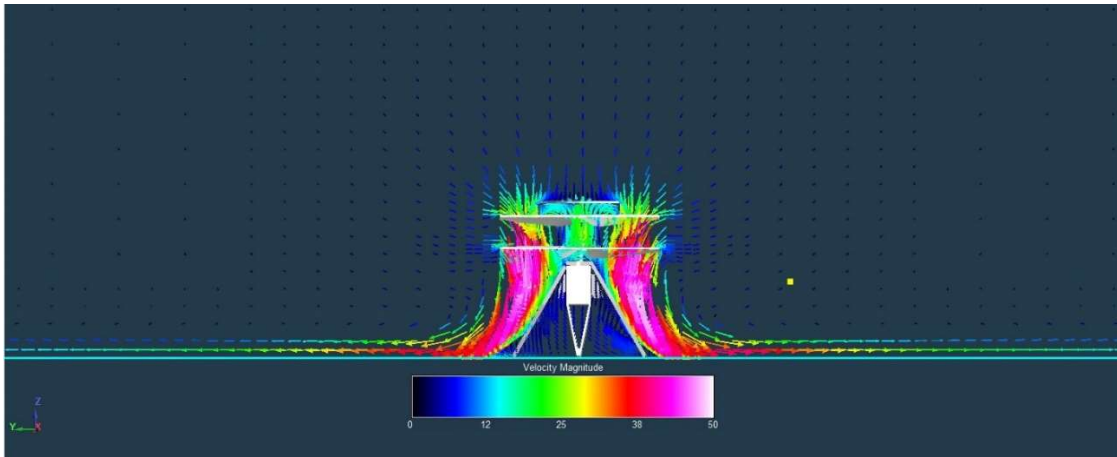
Figure 25. CFD flow field prediction of hover in ground effect (HIGE) – landing legs on the ground -- with circular solar array disk mounted above the upper rotor

With larger, heavier vehicles operating with higher tip speeds and disk loadings to compensate for the lower atmospheric densities of the Martian highlands, it is necessary to reexamine some of the early concerns for the Ingenuity Mars Helicopter Technology Demonstrator, including dust kick-up during takeoff and landing.
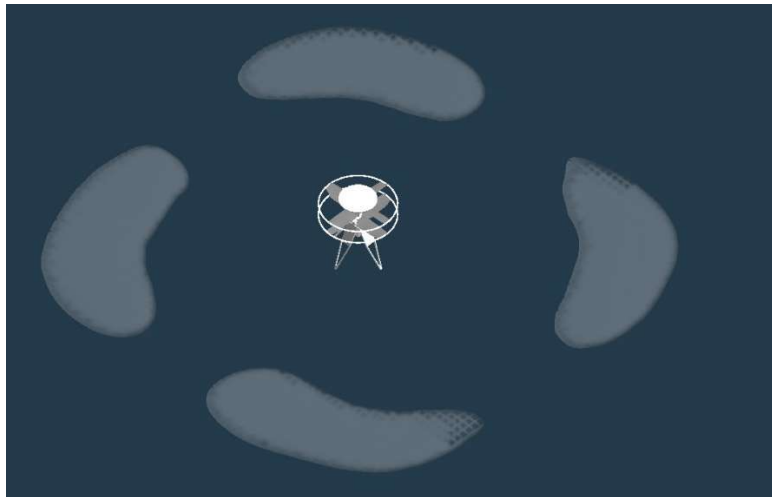

Figure 26. Representative preliminary dust kick-up predictions for HIGE operation (isosurfaces of dust density)

Two different airfoil sets have been optimally designed and discussed in Refs. 4, 13, and 14. The first set of airfoils is based upon cambered circular-arc airfoils. These airfoils were analytically shown to have significant improvements over the AeroVironment-developed CLF5605 airfoil used for the Ingenuity Mars Helicopter Technology Demonstrator, as documented in Ref. 13. A more recent set of airfoils, employing diamond- and triangular-shaped geometries as well as 'kinked' flat-plate airfoils, have been computationaly shown to perform better than the earlier generation of cambered circular-arc airfoils, Ref. 14. Figure 27 presents the relative figure-of-merit curves predicted by RotCFD for a notional 2m diameter Mars Highland Helicopter for rotors incorporating the first set of circular-arc airfoil decks. Future work will consider the more

recent low-Reynolds number airfoils. These initial hover performance results are for closely-spaced rotor-to-rotor separation distance of s/R=0.125.
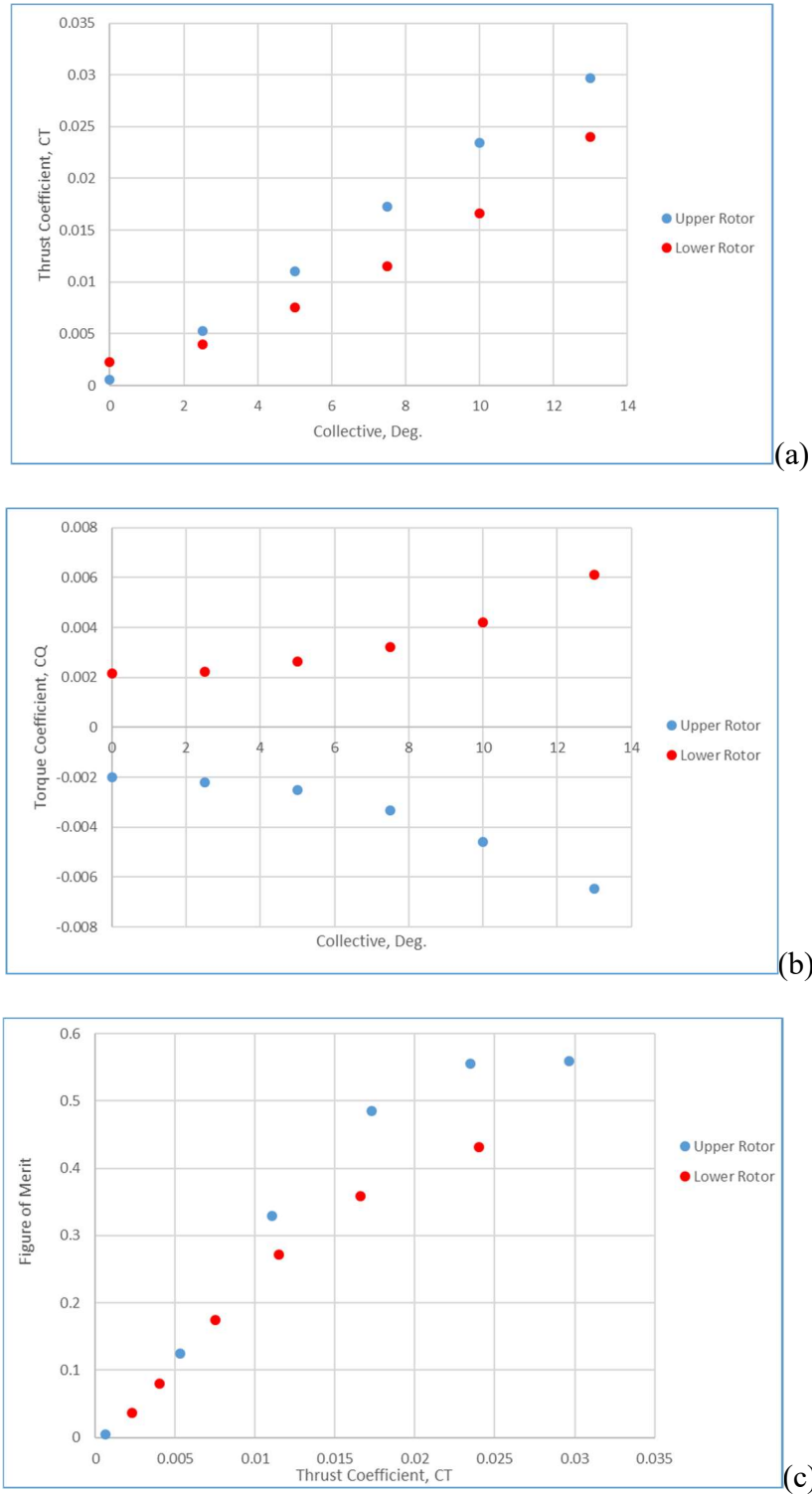

(a)

(b)

(c)

Figure 27. Coaxial rotor hover performance curves: (a) C_T vs. collective; (b) C_Q vs. collective; (c) figure-of-merit vs. C_T

The above results are for coaxial rotors (rotors only) with closely spaced rotors (s/R =0.125) in hover. The following results are provided for a complete vehicle configuration (including the fuselage and solar disk array). This configuration includes a relatively large rotor-to-rotor spacing (s/R = 0.4). Additionally, the solar disk is fairly large and in close proximity to the upper rotor (s_d/R = 0.2). The Mars Helicopter Technology Demonstrator, Ingenuity, initially considered a solar disk array but ultimately incorporated a rectangular array. Ingenuity flies relatively slowly. Accordingly, the aerodynamic interference effects of the rotor-mounted solar array on Ingenuity were relatively small. Because MHH is intended to fly at higher speeds, with a design target of 30m/s for maximum edgewise forward-flight cruise speed, the anticipation is that the solar array aerodynamic interference effects might be larger than that of Ingenuity.
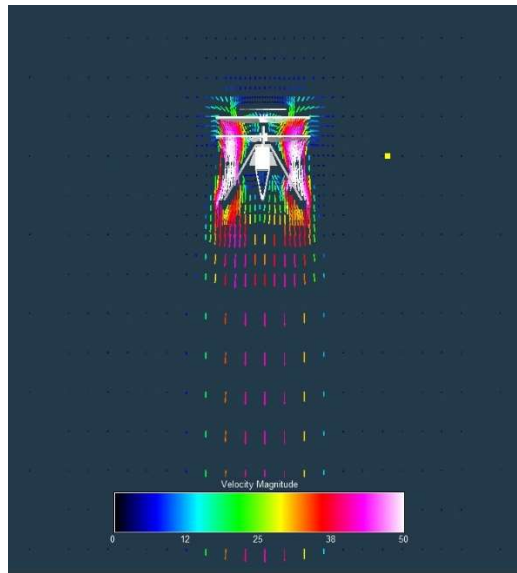

Figure 28. CFD flow field prediction of hover out of ground effect (HOGE) with circular solar array disk mounted above the upper rotor
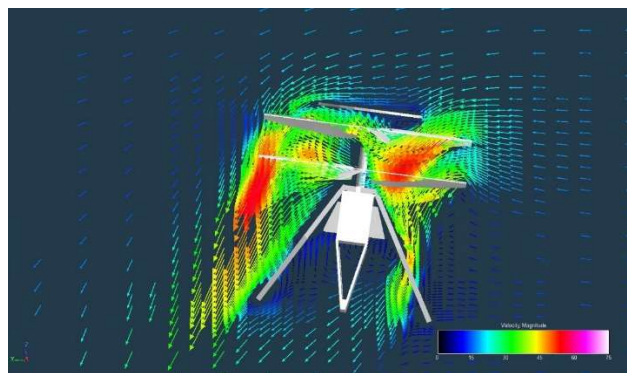

Figure 29. RotCFD flow field predictions of MHH forward flight (Coll. = 15 Deg. for both rotors; A_{shaft} = 7.5 Deg. nosedown; V = 15 m/s

Figure 30a-c are preliminary forward-flight predictions for the 2m rotor diameter MHH configuration with fuselage and with and without solar disk array with the rotor collectives at 15

33

Deg. These predictions are for a larger rotor-to-rotor spacing of s/R=0.4. The rotor-to-rotor spacing seems to have a significant impact on rotor thrust and power coefficients as compared to results for much closer rotor-to-rotor spacings. The collective settings for both rotors are at 15 Deg; therefore, the rotors are not torque balanced in this initial set of results. No cyclic control or vehicle attitude trim are applied in these initial results as well. The prescribed vehicle attitude varies as $\alpha_{Shaft} = 15V/30$. (Fuselage drag results after this initial set of predictions would suggest that the vehicle nosedown attitude is over-prescribed and that the α_{Sha} values need to be reduced for follow-on predictions.) Figure 30a shows the variation of thrust coefficients as a function of advance ratio (V/V$_{Tip}$). Figure 30b shows the trend of power coefficients with advance ratio. Figure 30c presents the rotor power-loading, C_T/C_P; power-loading is a measure of the rotor efficiency with operating condition. Power-loading is, overall, low for MHH (and Mars rotorcraft, in general) but trends do show the anticipated increase in power loading as hover is approached.

(a)

(b)

34

(c)
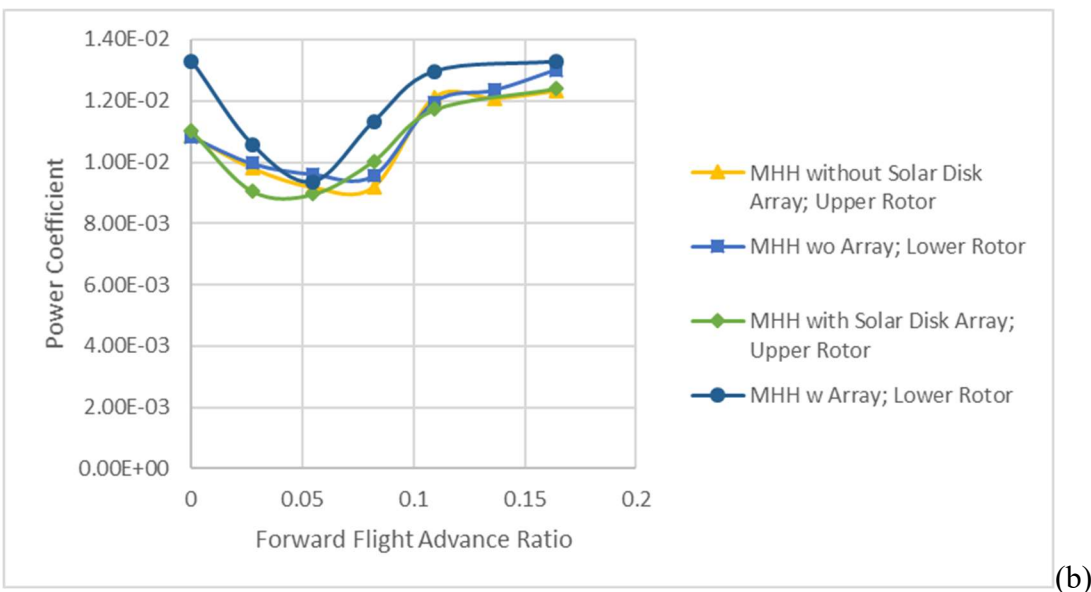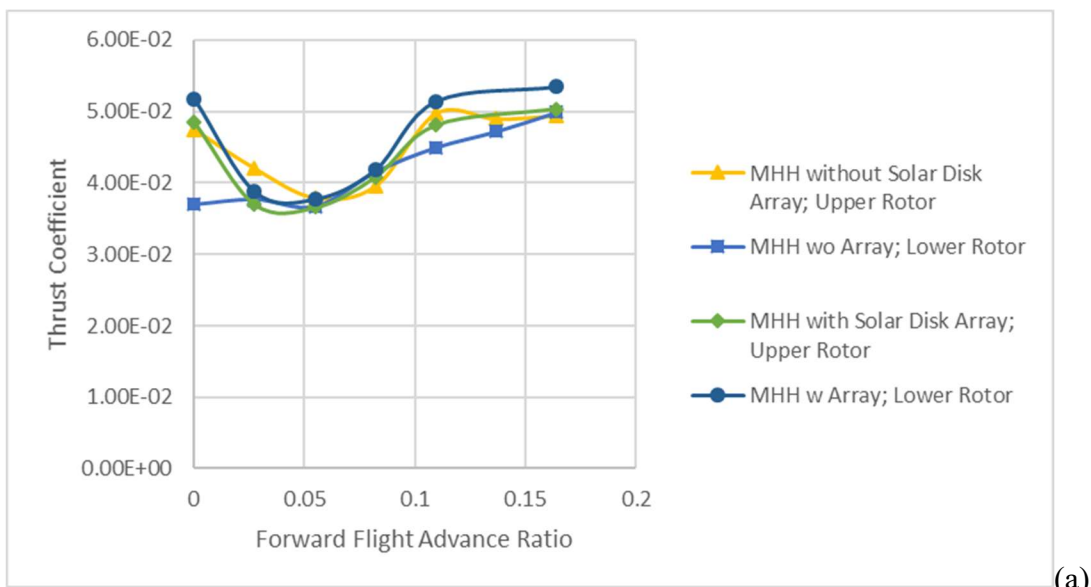
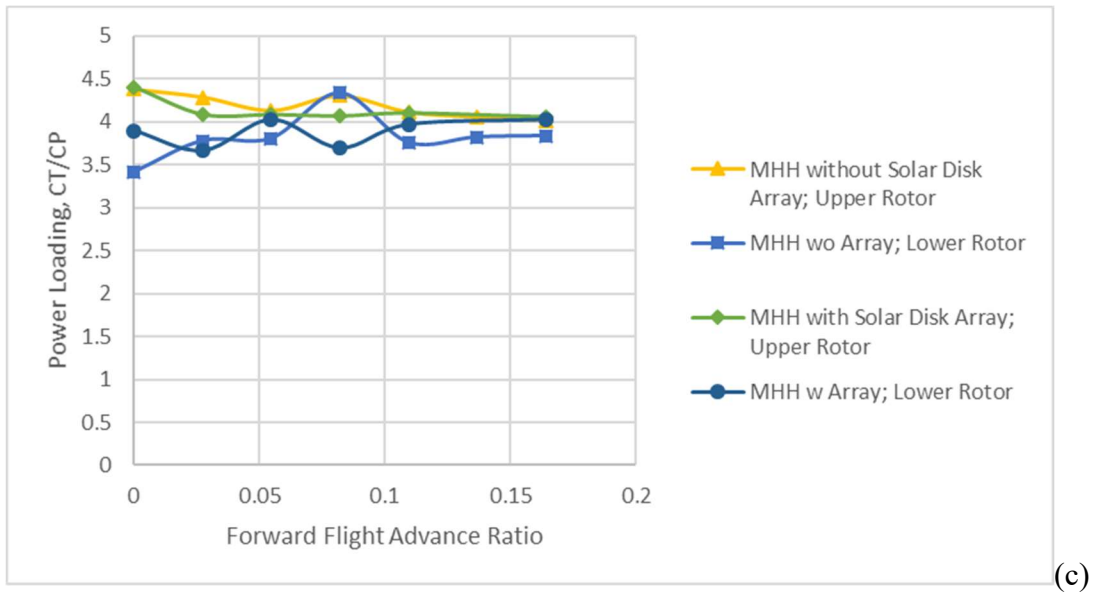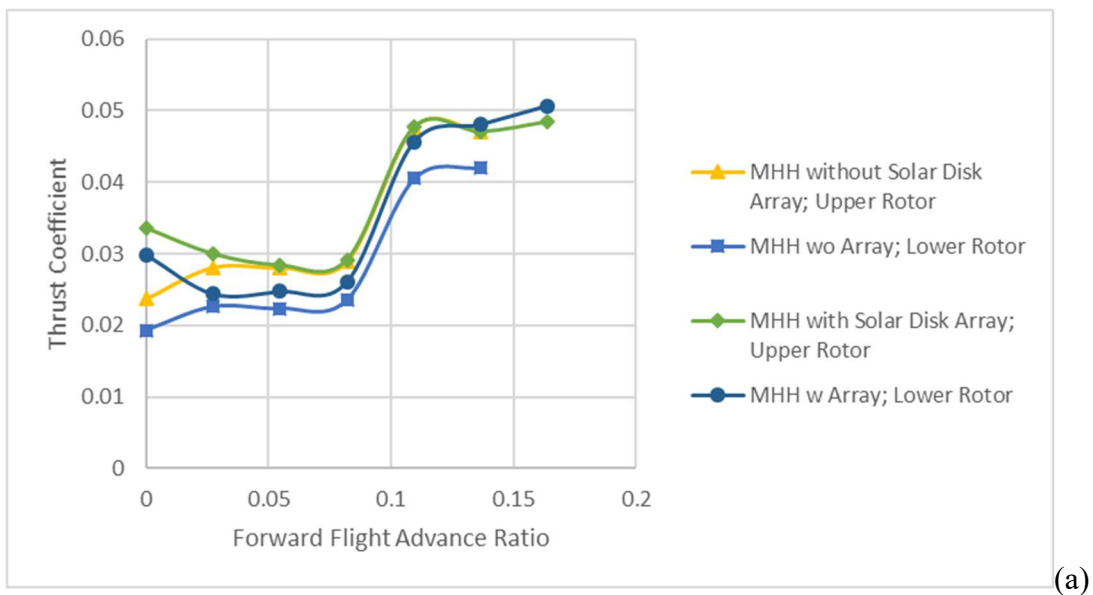**Figure 30.   RotCFD predictions of one MHH forward flight performance (collective = 15Deg. and s/R=0.4): (a) CT vs. advance ratio, (b) CP vs. advance ratio, and power-loading (C_T/C_P) vs. advance ratio**

Figure 31a-b is another set of forward flight performance predictions for a second MHH configuration, where the s/R=0.125 and, consequently, both rotors are limited to a collective of 13 Deg.
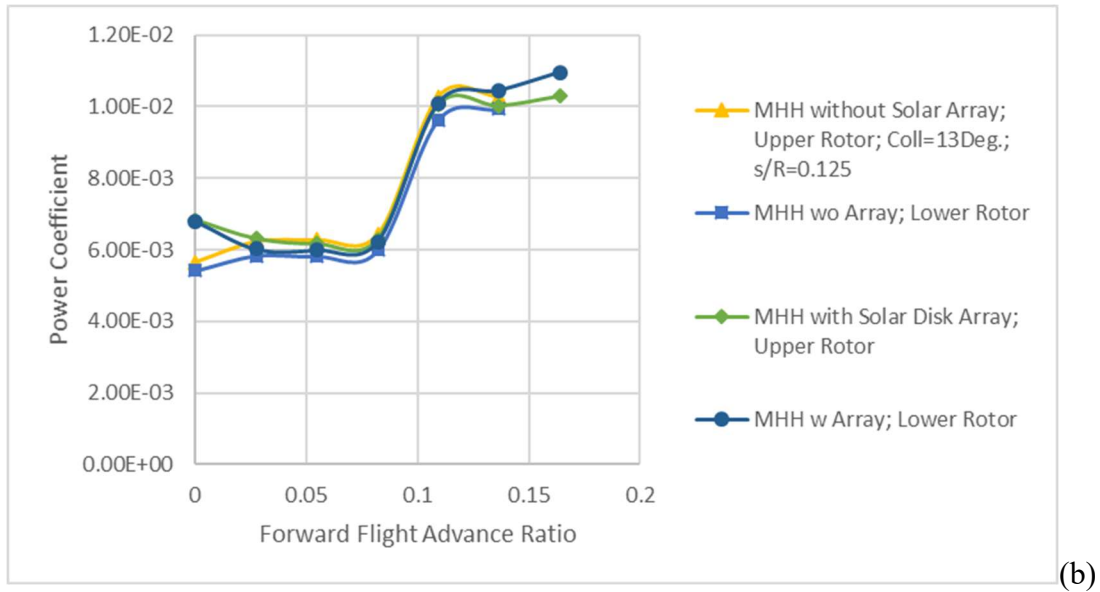

(a)

(b)

Figure 31.   RotCFD predictions of second MHH forward flight performance (fixed collective for both rotors = 13Deg. and s/R=0.125): (a) CT vs. advance ratio and (b) CP vs. advance ratio

Possible Mechanical Design Implementations of Stowable Vehicle

Forming a thin 'pancake' volume for stowed MHH vehicles is essential.   Rotor blades cannot be folded or canted into more compact volumes because of the operational challenges of spinning up and deploying the aircraft dictated by mid-air-deployment.   The notional vehicle fuselage design incorporates more than folding legs that fall within the 'pancake' stowed volume when fully folded; instead, this early design concept proposes the landing legs to be integrated into a 'flat sat' set of four avionics/science instrument packages.   These integral landing-leg/avionics packages would incorporate their own electronics, instruments, and a portion of the overall batteries and power electronics necessary to opperate the electric drive motors of the rotors and the servos for the rotor control systems.   This approach would potentially result in the most comfortable overall stowed volume to fit within the aeroshell. The downside of this approach is that all of these individual avionics packages will have to have their own insulation and survival heaters provided. This early design will be refined or superceded as the MHH project proceeds. Finally, as shown in Fig. 32, all four legs will be fully deployed prior to release from the aeroshell.
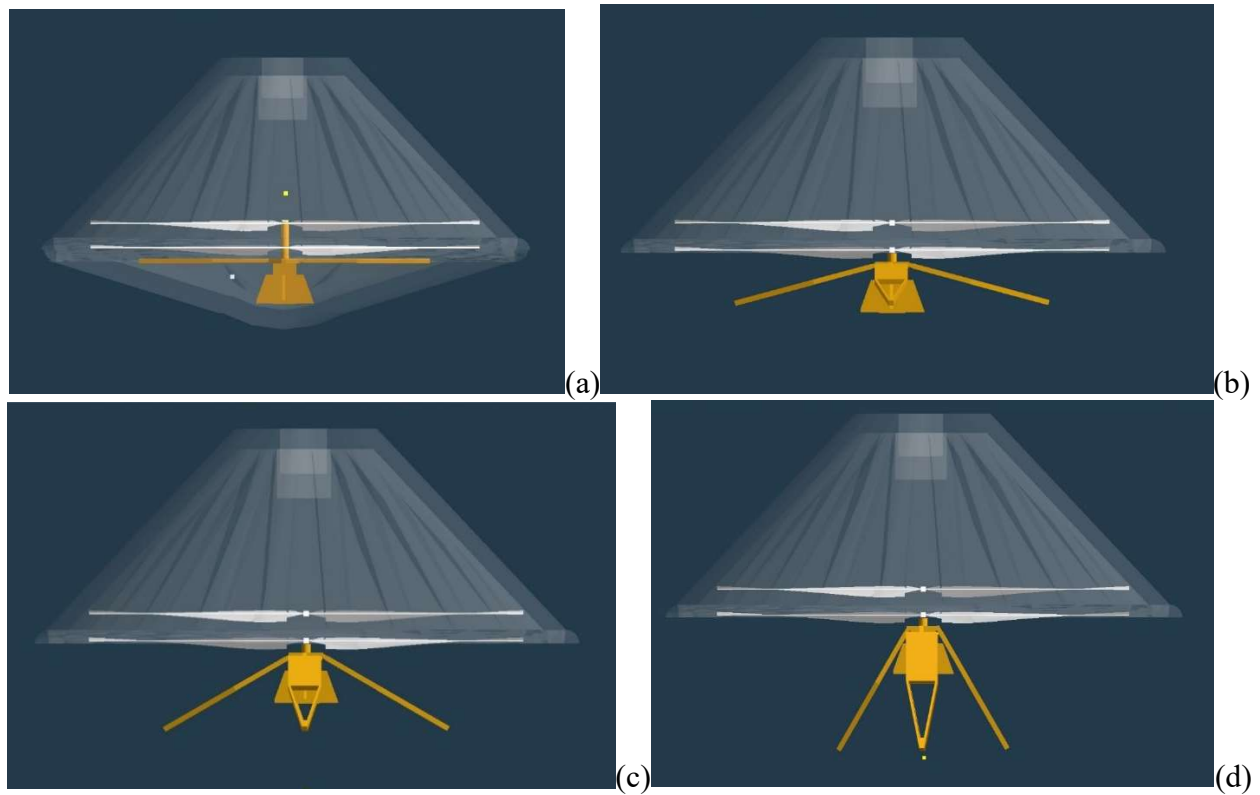
Figure 32. Deploying one possible (2m rotor diameter) MHH configuration: from (a) stowed to (d) fully deployed

Alternate, Smaller Vehicle Configurations

As can be readily seen above in Fig, 32 of the 2m diameter rotor baseline MHH design, it is challenging to package/stow this large of a rotor system in a Pathfinder-type aeroshell. To accommodate 2m diameter rotors, the rotor-to-rotor vertical separation between the two coaxial rotors needs to be reduced to a very small spacing, which has resulting performance and control implications. The rotor collective range may need to be reduced below maximum rotor thrust capability, and/or it might be required to increase blade-root cutouts or increase blade root inverse tapering, both of which would reduce much needed blade area/solidity. Alternatively, it might be required to consider smaller sized rotors to better fit within a Pathfinder-class aeroshell. Reference 19 details a new Ingenuity-class Mars design called the Advanced Mars Helicopter (AMH). This AMH was examined as a starting point for a smaller 1.2m diameter Mars Highland Helicopter.

Figure 33. Improvements of a small MHH vehicle as compared to the Ingenuity Mars Helicopter Technology Demonstrator

Table 1. Performance details from NDARC sizing of the 1.21m diameter rotor MHH

|		MAD
design C_T/σ		0.095
maximum C_T/σ		0.161
design M_{tip}		0.8
MAD M_{tip}		0.85
design density	kg/m³	0.01
design temp	C	-59
speed of sound	m/sec	228.28
cruise speed	m/sec	30
payload	kg	0.54
rotor radius	m	0.605
gross weight	kg	4.141
number of rotors		2
number of blades		4
disk loading	kg/m²	3.60
wake velocity v_h	m/sec	25.8
solidity		0.404
tip speed	m/sec	183
rotor speed	rpm	2882
total power	kW	0.89
max power	kW	1.33
max torque	Nm	4.41
battery (usable)	Ah	32.2
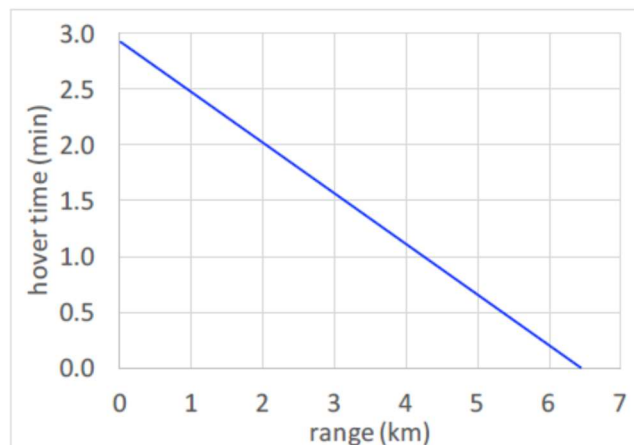
Figure 34. NDARC estimates of the tradeoff of hover time (minutes) versus range (kilometers) for the 1.21m rotor diameter MHH

Descent estimates were made in Ref. 6 for the smaller MHH conceptual design. A summary set of descent profiles is reproduced below from that paper, Fig. 35, for the reference design outlined in Table 1.
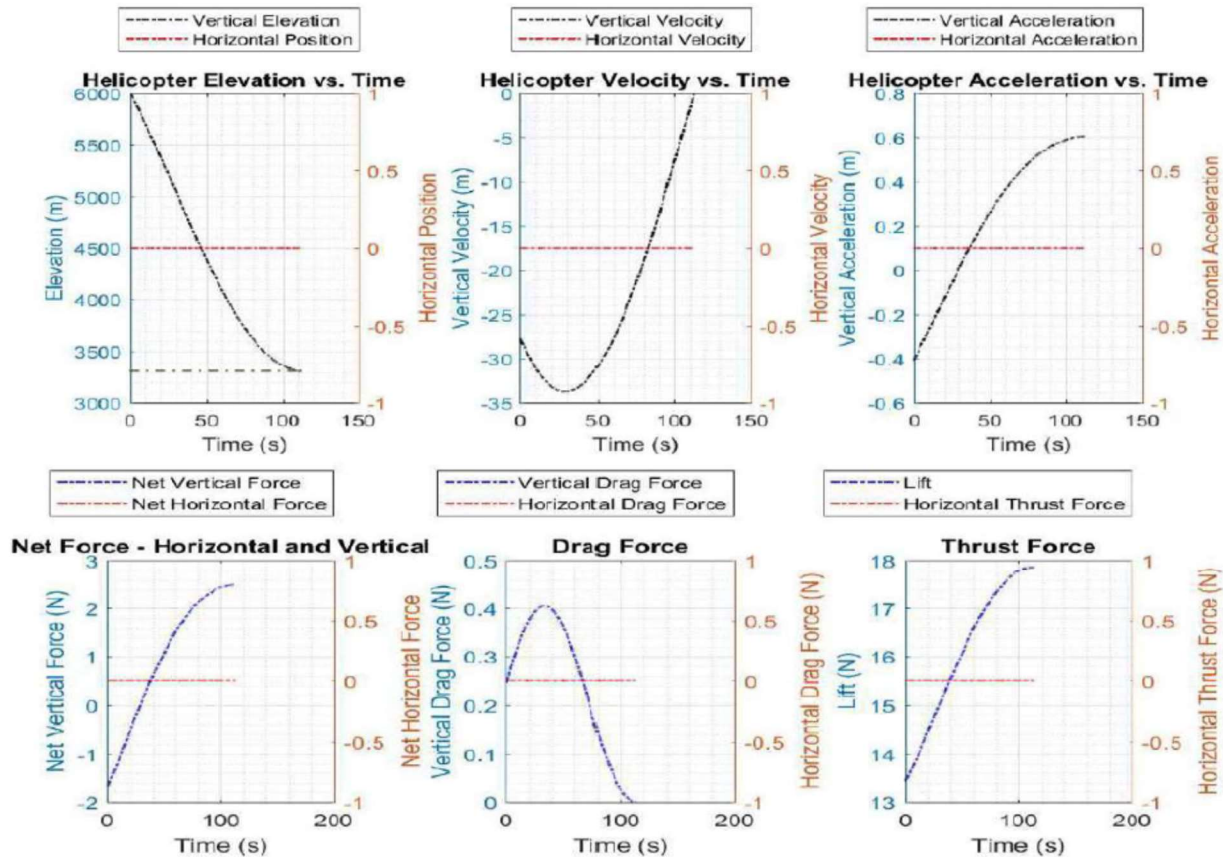

Figure 35. Mid-air-deployment descent profiles from classic extended-momentum-theory and blade element analysis (results from Ref. 6)

Concluding Remarks

Flying over the Martian highlands with the higher altitudes – and significantly lower atmospheric densities and much colder temperatures – will require an additional level of design challenges for Mars helicopters and other rotorcraft. A Mars Highland Helicopter (MHH) will build upon the success of the Ingenuity Mars Helicopter Technology Demonstrator and, perhaps, other follow-on vertical takeoff and landing aerial vehicles. However, because of the challenges of flight over the Martian highlands, the MHH design will be a mix of both the familiar and the radically different.

This paper is a preliminary study. It and a companion mission-definition paper are the first attempts to define the Mars Highland Helicopter mssion concept, science rationale, and vehicle conceptual design. A considerable amount of follow-on work is required to one day see the realization of the MHH mission. Further, the flexibility of Mars rotorcraft to perform planetary

science campaigns, and to potentially support human missions to Mars, means that there will likely be several competing Mars rotorcraft mission proposals to consider in the future as natural successors to a successful Ingenuity Mars Helicopter Technology Demonstrator. Ingenuity took over five years to develop. Though there is likely considerable design heritage stemming from Ingenuity to MHH – and other concepts such as the complementary JPL/Ames Mars Science Helicopter (MSH) development effort – there will also likely be a significant amount of development work that will be required to examine the unique technical challenges of the mid-air-deployment and VTOL flight over the Martian highlands.

Acknowledgments

References

[1]Young, L. A., Chen, R. T. N., Aiken, E. W., Briggs, G. A., "Design Opportunities and Challenges in the Development of Vertical Lift Planetary Aerial Vehicles," Proceedings of the American Helicopter Society International Vertical Lift Aircraft Design Conference, San Francisco, CA, January 2000.

[2]Delaune, J., et al, "Enabling Mars Highlands Exploration By a Mid-Air-Deployed Helicopter," AIAA ASCEND, September 2020.

[3]Withrow-Maser, S., Koning W., Kuang W., Johnson, W., "Recent Efforts Enabling Future Mars Rotorcraft Missions," Presented at the VFS Aeromechanics for Advanced Vertical Flight Technical Meeting, San Jose, CA, January 21–23, 2020

[4]Koning, W.J.F, Johnson, W., and Grip, H.F., "Improved Mars Helicopter Aerodynamic Rotor Model for Comprehensive Analyses," AIAA Journal, Vol. 57, No. 9, September 2019.

[5]Rapin, W., et al, "Critical knowledge gaps in the Martian geological record:A rationale for regional-scale in situ exploration by rotorcraft mid-air deployment," Science White Paper for the NASEM Planetary Science Decadal Survey (PSDS), June 2020.

[6]Bhagwat, R.S., Johnson, W., and Withrow, S. , "High Altitude Deployment of a Science Rotorcraft on Mars," NASA Internship Report, May 1, 2020.

[7]Rajagopalan, R.G., Baskaran,V., Hollingsworth, A., Lestari, A., Garrick, D., Solis, E., Hagerty, B., "RotCFD - A Tool for Aerodynamic Interference of Rotors:Validation and Capabilities", AHS Future Vertical Lift Aircraft Design Conference, January 18-20, 2012, San Francisco.

[8]Young, L., Yamauchi, G., Rajagopalan, G., "Simulated Rotor Wake Interactions Resulting from Civil Tiltrotor Aircraft Operations Near Vertiport Terminals," AIAA 2013.

[9]Perez Perez, B.N., "Forward Flight Rotor Performance at Martian Atmospheric Densities and Sensitivity to Low Reynolds Numbers," Presented at the VFS Aeromechanics for Advanced Vertical Flight Technical Meeting, San Jose, CA, January 21–23, 2020.

[10]Grip, H., Johnson, W., Malpica, C., Scharf, D., Mandic, M., Young, L., Allany, B., Mettlerz, B., San Martin, M., "Flight Dynamics of a Mars Helicopter," 43rd European Rotorcraft Forum, Milan, Italy, September 12-15, 2017.

[11]Johnson, W., "Model for Vortex Ring State Influence on Rotorcraft Flight Dynamics," Proceedings of the American Helicopter Society 4th Decennial Specialists' Conference on Aeromechanics, San Francisco, California, January 21-23, 2004.

[12]Young, L.A., Briggs, G., Aiken, E., and Pisanich, G., "Rotary-Wing Decelerators for Probe Descent through the Atmosphere of Venus," 2nd International Planetary Probe Workshop, NASA Ames Research Center, Moffett Field, CA, August 2004 (NASA CP-2004-213456, April 2005).

[13]Koning, W.J.F., Romander, E., Johnson, W., "Performance Optimization of Plate Airfoils for Martian Rotor Applications Using a Genetic Algorithm," Presented at the 45th European Rotorcraft Forum, Warsaw, Poland, 17-20 September, 2019.

[14]Koning, W.J.F., Romander, E.A., Johnson, W., "Optimization of Low Reynolds Number Airfoils for Martian Rotor Applications Using an Evolutionary Algorithm" Presented at the AIAA Science and Technology Forum and Exposition (AIAA SciTech), Orlando, Florida, USA, January 6–10, 2020.

[15]Levin, A.D. and Smith, R.C., "Experimental Aerodynamics of a Rotor Entry Vehicle," 3rd AIAA Aerodynamic Decelerator Systems Technology Conference, El Centro, CA, September 23-25, 1968, Technical Report NO. 69-11 April 1969.

[16]Levin, A. D. and Smith, R. C., "Experimental aerodynamic performance characteristics of a rotor entry vehicle configuration. 1 – Subsonic," NASA-TN-D-7046, 1971.

[17]Giansante, N. and Lemnios, A. Z., "The dynamic behavior of rotor entry vehicle configurations. Volume 1 - Equations of motion," NASA-CR-73390, 1968.

[18]Mars Atmosphere Model; https://www.grc.nasa.gov/WWW/K-12/airplane/atmosmrm.html; last accessed September 26, 2020.

[19]Withrow-Maser, S., Johnson, W., Young, L., Cummings, H., Chan, A., Balaram, J., Tzanetos, T., "An Advanced Mars Helicopter Design," AIAA ASCEND Conference, November 16-18, 2020.